HHS Public Access

Author manuscript

Harmful Algae. Author manuscript; available in PMC 2025 April 14.

Published in final edited form as:

Harmful Algae. 2025 April ; 144: 102834. doi:10.1016/j.hal.2025.102834.

Growth and anatoxin-a production of *Microcoleus* (Cyanobacteria) strains from streams in California, USA

Sydney M. Brown[a,b], **Joanna R. Blaszczak**[c], **Robert K. Shriver**[c], **R.Christian Jones**[a,b], **Abeer Sohrab**[d], **Ramesh Goel**[d], **Gregory L. Boyer**[e], **Bofan Wei**[e], **Kalina M. Manoylov**[f], **T.Reid Nelson**[a,b], **Jordan M. Zabrecky**[c], **Rosalina Stancheva**[a,b,*]

[a]Department of Environmental Science and Policy, George Mason University, Fairfax, VA 22030, USA

[b]Potomac Environmental Research and Education Center, Woodbridge, VA 22191, USA

[c]Department of Natural Resources and Environmental Science, University of Nevada, Reno, NV, USA

[d]Department of Civil and Environmental Engineering, University of Utah, Salt Lake City, UT 84112, USA

[e]Department of Chemistry, State University of New York College of Environmental Science and Forestry, Syracuse, New York, USA

[f]Department of Biological and Environmental Sciences, Georgia College & State University, Milledgeville, GA, USA

*Corresponding author: rchris13@gmu.edu (R. Stancheva).

Declaration of competing interest

The authors declare the following financial interests/personal relationships which may be considered as potential competing interests: Gregory Boyer reports financial support was provided by National Institute of Environmental Health Sciences. Sydney Brown reports financial support was provided by National Science Foundation. Gregory Boyer reports financial support was provided by National Science Foundation. Rosalina Stancheva reports financial support was provided by National Science Foundation. Ramesh Goel reports financial support was provided by National Science Foundation. Abeer Sohrab reports financial support was provided by National Science Foundation. Joanna R. Blaszczak reports financial support was provided by National Science Foundation. Robert K. Shriver reports financial support was provided by National Science Foundation. Jordan Zabrecky reports financial support was provided by National Science Foundation. If there are other authors, they declare that they have no known competing financial interests or personal relationships that could have appeared to influence the work reported in this paper.

CRediT authorship contribution statement

Sydney M. Brown: Writing – review & editing, Writing – original draft, Visualization, Methodology, Investigation, Formal analysis, Data curation, Conceptualization. **Joanna R. Blaszczak:** Writing – review & editing, Writing – original draft, Resources, Funding acquisition, Data curation. **Robert K. Shriver:** Writing – review & editing, Writing – original draft, Visualization, Funding acquisition, Formal analysis, Data curation, Conceptualization. **R.Christian Jones:** Writing – review & editing, Writing – original draft, Formal analysis, Data curation. **Abeer Sohrab:** Writing – review & editing, Writing – original draft, Methodology, Investigation, Formal analysis, Data curation. **Ramesh Goel:** Writing – review & editing, Writing – original draft, Supervision, Funding acquisition, Formal analysis, Data curation. **Gregory L. Boyer:** Writing – review & editing, Writing – original draft, Supervision, Methodology, Formal analysis, Data curation. **Bofan Wei:** Formal analysis, Data curation. **Kalina M. Manoylov:** Writing – review & editing, Writing – original draft, Supervision, Methodology, Formal analysis, Data curation. **T.Reid Nelson:** Formal analysis. **Jordan M. Zabrecky:** Writing – review & editing, Writing – original draft, Data curation. **Rosalina Stancheva:** Writing – review & editing, Writing – original draft, Visualization, Supervision, Resources, Methodology, Investigation, Funding acquisition, Data curation, Conceptualization.

Supplementary materials

Supplementary material associated with this article can be found, in the online version, at doi:10.1016/j.hal.2025.102834.

Abstract

Benthic cyanobacterial proliferations are an emerging concern globally due to their potential for toxin production and subsequent negative environmental and health impacts. *Microcoleus* is a common mat-forming genus reported to produce potent neurotoxin, anatoxin-a, ingestion of which has been associated with animal mortalities. Six different unialgal monoclonal strains of *Microcoleus* were isolated from streams in California and grown in batch culture for 49 days. The four toxic strains were identified using a polyphasic approach as belonging to the species *Microcoleus anatoxicus*, which expands its known distribution throughout the Klamath River and Rock Creek watersheds in northern California. The non-toxic strains from the Eel River belonged to *Microcoleus* sp. 1. Maximum toxin production occurred during the exponential growth phase, and peaked 6–13 days later in more toxic strains, with a persistently higher fraction of extracellular toxins compared to less toxic strains, which had maximum toxin concentrations at day 13. The proposed mechanism of toxin release into culture medium was through damage to the cell walls of unhealthy filaments. Peak toxin production was energetically expensive for all *M. anatoxicus* strains, evidenced by reduced specific growth rates at the time of peak toxin production, followed by quick recovery of cell division. Despite this, more toxic strains achieved faster maximum growth rates than the less toxic and non-toxic strains under luxurious nutrient culture conditions. Differential toxin and growth rate responses of *M. anatoxicus* strains from wide geographical ranges under the same laboratory-controlled conditions suggest high intraspecific variation, which may represent challenges for harmful algal blooms mitigation. More toxic strains have the potential to proliferate and consistently release extracellular anatoxins into the environment. This study provides a baseline to understanding the growth and toxin kinetics of two commonly occurring *Microcoleus* species in northern California which may help benthic harmful cyanobacteria management.

Keywords

Microcoleus ; Streams; Anatoxin-a; Growth rate; Chlorophyll-*a*; Cyanobacteria

1. Introduction

Cyanobacterial blooms are increasing globally with detrimental effect on aquatic ecosystems and water quality through production of cyanotoxins and nuisance biomass (Pearl et al., 2001; Huisman et al., 2018; Amorim et al., 2021). However, most of our understanding of harmful blooms is focused on planktonic cyanobacteria while benthic taxa have remained relatively understudied (Quiblier et al., 2013; Wood et al., 2020). Representatives of *Microcoleus* Desmazières ex Gomont, a sheathed filamentous cyanobacteria, commonly form benthic mats in streams, rivers and lake beds (Komárek and Anagnostidis, 2005; Strunecký et al., 2013; Wood et al., 2012, 2020; McAllister et al., 2016). Recently, widespread proliferations of *Microcoleus* are environmental concern because of their potential to produce cyanotoxins (Wood et al., 2012, 2020). Some *Microcoleus* species can produce potent neurotoxins, collectively known as anatoxins (Heath et al., 2010; Wood et al., 2018; Bouma-Gregson et al., 2019), encoded by the *Ana* gene cluster (Méjean et al., 2009, 2010, 2014; 2016; Conklin et al., 2020; Kust et al., 2020). Anatoxins are non-

ribosomally synthesized alkaloids which bind the acetylcholine receptor. When ingested, this can result in death via respiratory paralysis (van Appeldorn et al., 2007; Méjean et al., 2009). There are multiple common congeners of anatoxin-a with varying toxicities, including anatoxin-a (ATX), α and β-dihydroanatoxin-a (dhATX), homoanatoxin-a (HTX), and α and β-dihydrohomoanatoxin-a (dhHTX).

Anatoxins are of an environmental concern for their toxicity on aquatic organisms and domestic animals that incidentally ingest mats. Anatoxins have been identified as the cause of dog deaths globally (Hamill, 2001; Gugger et al., 2005; Wood et al., 2007; Puschner et al., 2008; Bouma-Gregson et al., 2018; Valadez-Cano et al., 2023; Johnston et al., 2024; Junier et al., 2024). Crude extracts containing anatoxins from *Microcoleus* cultures were toxic to three macroinvertebrates (*Ceriodaphnia dubia, Hyalella azteca*, and *Chironomus dilutus*) at naturally occurring environmental concentrations (Anderson et al., 2018). However, a subsequent study has found that purified anatoxins did not cause lethal effect on larvae of the aquatic mayfly, *Deleatidium* spp. (Kelly et al., 2020) indicating possible presence of unidentified toxins in the mats. In laboratory studies conducted on mice, dhATX was reported to be more potent than ATX by the oral route (Puddick et al., 2021), however, research is still lacking on HTX and dhHTX toxicity in relation to other anatoxin congeners. In the environment, toxigenic *Microcoleus* species can vary in relative abundances which ultimately affects mat toxin concentrations (Heath et al., 2010; Wood and Puddick, 2017; Kelly et al., 2019). However, little is known about which drivers promote the proliferation of toxigenic genotypes. Additionally, the biological function of anatoxins remains to be established (Holland and Kinnear, 2013), with no understanding of the physiological or ecological advantages to the energetically expensive production of this molecule.

In northern California, in the summertime, *Microcoleus* dominates benthic mats in the South Fork of the Eel River (Bouma-Gregson et al., 2019; 2021), the Russian River and its tributaries (Conklin et al., 2020; Bouma-Gregson et al., 2021) and the streams within the Klamath River watershed (Genzoli et al., 2024). In the Eel River, Bouma-Gregson et al. (2019) detected four different and novel *Microcoleus* genotypes, three of which were non-toxic, but only one species was wide-spread throughout the watershed tolerating variable nitrogen conditions and light levels (Bouma-Gregson et al., 2019). The toxic *Microcoleus* genotype detected in the Eel River (e.g., *Microcoleus* sp. 2; strains PH2015_14S_Oscillatoriales_45_132) was rare, occurred in locations where total dissolved nitrogen exceeded 70 μg/L, and was associated with a different non-cyanobacterial microbial community than its non-toxic counterparts (Bouma-Gregson et al., 2019). The toxic *Microcoleus* genotype was later detected in the Russian River (Bouma-Gregson et al., 2021) sharing a 99.9 % 16S rRNA sequence similarity to *M. anatoxicus* Stancheva & Conklin, which was isolated in 2015 and formally described from the same river following dog fatality (Conklin et al., 2020).

In the field, nutrient availability may influence *Microcoleus* growth and toxin production. Our non-toxic strains were isolated from the South Fork Eel River, where a historical presence of N_2-fixing algae has been recorded (Finlay et el., 2011; Weigel et al., 2020), highlighting low nitrogen concentrations in this river. *Microcoleus anatoxicus* persists in

nitrogen depleted culturing medium for long periods of time (Stancheva et al., 2024) confirming the wide nitrogen tolerance of this cyanobacterium. Furthermore, toxic strains have a higher predicted nitrogen need, potentially due to the nitrogen requirements to synthesize anatoxin-a (Tee et al., 2021). Field studies elucidated that low phosphorus concentrations coincide with *Microcoleus* blooms (McAllister et al., 2016) providing further evidence for the wide nutrient tolerances of this cyanobacterium. Researching strain-specific responses at a local scale is important to understand why different *Microcoleus* species dominate communities in different regions and if there are locally adapted environmental responses of *Microcoleus* taxa. For example, McAllister et al. (2018) in a field study of several streams in New Zealand determined that *Microcoleus* cover and toxin concentrations were highly variable both spatially and temporally. The specific site was a strong explanatory variable, indicating that different strains may influence the toxin content of a mats and their growth (McAllister et al., 2018).

The genus *Microcoleus* represents a continuum consisting of a minimum of 12 distinct species with varying levels of gene flow and divergence (Skoupý et al., 2024). *Microcoleus* species from California could differ genetically and eco-physiologically from their New Zealand's counterparts being adapted to different climatic and environmental conditions. Better understanding of species diversity, biomass accrual and timing of the toxin production at local scale allows development of regional management programs because robust prediction tools of *Microcoleus* growth are difficult to construct (McAllister et al., 2018).

Here, we studied under laboratory conditions four toxic and two non-toxic *Microcoleus* strains isolated from four stream watersheds in northern California. The toxic *Microcoleus* strains in this study produced different congeners and concentrations of anatoxins. We tested whether the production of different anatoxin congeners and/or concentrations of toxins produced affect *Microcoleus* growth rates. We also determined if *Microcoleus* species from California exhibit similar responses as the strains isolated from New Zealand. We are interested in the growth rates of the toxic and non-toxic *Microcoleus* species to build a framework to better understand how toxin production and mat development varies in laboratory conditions and its ecological relevance to northern California watersheds. Previously, Heath et al. (2016) reported the growth rates for *Microcoleus* strains isolated from New Zealand streams was higher for the non-toxic strain compared to the toxic strain across varying nutrient treatments at environmentally relevant conditions, but we do not know if this is universally true and applicable to *Microcoleus* species growing in California under different climate conditions.

The goals of this research were to 1) analyze the phylogenetic relationship of *Microcoleus* species isolated from streams in northern California to other strains around the globe; 2) assess and compare growth rates of toxigenic *Microcoleus* strains producing different anatoxin congeners and concentrations with non-toxigenic *Microcoleus* strains, and 3) identify periods of peak toxin production during growth trajectories and how that relates to time-specific growth rate and cellular responses. We expected that the toxic and non-toxic strains used for the experiments would be phylogenetically distant and would group into two separate phylogenetic clades, as previously demonstrated by genomic analysis of 42 *Microcoleus* strains, including *M. anatoxicus* (Tee et al., 2021). As toxins are energetically

expensive to produce and are involved in nutrient metabolic processes (Tee et al., 2021), we hypothesized that toxigenic *M. anatoxicus* strains would have slower maximum growth rates than their non-toxic counterparts as previously reported for *Phormidium* (presumably *Microcoleus*) strains (Heath et al., 2014; 2016), as well as slower growth rates for strains producing two anatoxin congeners (ATX and dhATX) versus one (dhATX). We also hypothesized that toxin production would have a negative effect on cell growth during periods of peak toxin production, evidenced through specific growth rates between each harvest.

2. Materials and methods

2.1. Cyanobacteria strain isolation and culturing

In this study, we used six different *Microcoleus* strains with varying toxin-producing capabilities which were isolated from four stream watersheds in northern California between 2015 and 2022 (Fig. 1, Table 1). We isolated additional monoclonal *Microcoleus* strains from each field sample as described in Conklin et al. (2020). Briefly, strain isolation and culturing were performed on solid and liquid BG11 medium (Sigma-Aldrich, St. Louis, MO). Filaments were transferred to a new solid medium multiple times over the course of several months until monoclonal culture was obtained by isolating the tip of single trichome grown on solid BG11, which took several months. All strains used in this study were unialgal, monoclonal, and non-axenic, which was confirmed by sequencing the metagenome of each culture (see Section 2.3 below). Strains were maintained long-term in liquid BG11 medium with a pH of 7.2 under 21 °C with an irradiance of 100 μmoles/m^2/s and a 12:12 hr light:dark cycle and transferred into fresh media every 45–60 days until the start of the experiment.

Microcoleus anatoxicus strain PTRS1 was previously isolated from the coastal Russian River, state site Camp Rose #114RR3119 on October 1, 2015 as described in Conklin et al. (2020). Initially, this strain produced both detectable ATX and dhATXs, but over time it no longer produced detectable ATX in laboratory conditions. *Microcoleus anatoxicus* strain RC9 was isolated on October 7, 2020 from Rock Creek, which is a hot spot for novel diatom diversity (Abarka et al., 2023; Stancheva, 2019; Mora et al., 2024) and located within the Southern Cascade Mountain Range. This strain only produced detectable dhATXs of the six monitored anatoxin-a congeners (see Section 2.7). *Microcoleus anatoxicus* strains SR16 and SR17 were isolated from the Scott River in the Klamath River Watershed, which is the most northern watershed in California, a historically eutrophic system (USGS, 2016). Both strains produce detectable ATX and dhATXs. *Microcoleus* sp. 1, represented by non-toxic strains ER6 and ER12, were isolated from the coastal South Fork Eel River draining the California Coast Range Mountains.

2.2. Experimental design

In this study, we used four anatoxin-a producing *Microcoleus* strains (e.g., *M. anatoxicus* strains PTRS1, RC9, SR16, SR17) and two non-toxic strains (e.g., *Microcoleus* sp. 1 strains ER6, ER12). We followed a method developed by Harland et al. (2013) to investigate changes in anatoxin quota in liquid cultures of benthic mat-forming cyanobacteria

(*Phormidium autumnale* strain CYN52). This method uses one set of triplicate samples to calculate the number of cells in the original 30 mL culture, and the biomass from a second triplicate sample set for anatoxin-a analysis. Then the anatoxin quota is calculated from these six individual technical replicates as fg/cell (Harland et al., 2013). The toxin quota is defined after Horst et al. (2014) as the amount of toxin per cell or per unit biomass. Toxin quota is a variable trait and can be a function of growth rate, culturing, and environmental conditions (Horst et al., 2014).

Prior to the experiment, all six *Microcoleus* strains were grown for 45 days in 125 mL Pyrex® glass Erlenmeyer flasks with 75 mL of liquid BG11 until reaching stationary phase and forming mats. *Microcoleus* filaments were gently removed with sterile microbiological loop from the sides of the flasks, and we split the initial inoculum into equal small clumps (approximately 4 mg) using visual estimation under sterile conditions.

A single clump was incubated in 30 mL Fisherbrand reusable borosilicate glass tubes (Thermo Fisher Scientific, Inc.) with 20 mL of BG11 medium, and grown for 49 days at 21 °C, under a light irradiance of 100 μmoles/m^2/s on a 12:12 light: dark cycle. We randomized and changed culture tube positions within the incubator at each harvest. Empty positions within the culture rack were filled with the same culture tubes filled with 20 mL of distilled water.

For each analysis described below replicates were grown in separate glass tubes. To analyze cell density, biovolumes, and physiological condition of filaments, triplicate cultures were grown and harvested at days 5, 8, 13, 15, 19, 26, 29, 33, 40, and 46, resulting in 165 individual cultures. At the day of the extraction, we preserved *Microcoleus* filaments by adding five to six drops of Lugol's iodine solution (Carolina Biological Science, Burlington, NC), and stored samples in the refrigerator at 4 °C.

To measure chlorophyll-*a* concentration, we harvested duplicate cultures at days 13, 19, 26, 33, 40, and 46, resulting in 72 individual cultures. To measure dry weight and toxin concentrations, we harvested duplicates of toxin-producing cultures (*M. anatoxicus* strains PTRS1, RC9, SR16, and SR17) at days 5, 13, 19, 26, 33, 40, and 46, resulting in 56 individual cultures. For molecular analysis, we grew each *Microcoleus* strain for twenty days as described above in 125 mL Pyrex® glass Erlenmeyer flasks with 75 mL of liquid BG11 to obtain enough biomass for DNA extraction. For morphological analysis of the filaments, we grew each *Microcoleus* strain for forty days as described above in 30 mL glass tubes.

2.3. Phylogenetic analyses

Microbial DNA was extracted from all samples using the Qaigen All Prep DNA/RNA kit (Cat. No. / ID: 80,284) following the manufacturer's kit instructions and measured its concentration with a Qubit Fluorometer at the University of Utah. Sequencing was done at the Huntsman Cancer Institute, University of Utah, using the Illumina NovaSeq X sequencer, producing 150 M base pair reads per sample. The quality of the reads was assessed using FastQC v0.11.8 (Andrews, 2010). The data were trimmed using Trimmomatic v0.38 (Bolger et al., 2014) applying a Phred quality score threshold of 24.

More than 90 % of the reads were retained after quality control. The high-quality, trimmed reads were assembled into contigs using CLC Genomic Workbench 23 developed by Qiagen. These contigs were used for binning with MetaBAT2 (Kang et al., 2019), grouping sequences likely from the same genome. The quality of the Metagenome-Assembled Genomes (MAGs) was evaluated using CheckM v1.0.7 (Parks et al., 2015), to assess contamination and completeness. Taxonomic classification was done using the Genome Taxonomy Database Toolkit (GTDB-Tk) (Chaumei, 2020). Maximum-likelihood trees were constructed with branch supports based on concatenated alignments of 120 single-copy core marker genes obtained from GTDB-Tk v0.2.1. For comparison, other reference genomes from diverse locations were also included in the phylogeny. These include reference *Microcoleus* genomes sourced from the Eel River watershed (Bouma-Gregson et al., 2019), Russian River (Conklin et al., 2020), Canada (Valadez-Cano et al., 2023), and New Zealand along with others documented in studies such as that by Tee et al. (2021) (See Supplement Table 1). The tree was rooted at midpoint with bootstrapping values greater than 50 % shown, indicating robustness. The tree was built using the ultrafast bootstrap approximation in IQ-TREE v1.6.9. (Nguyen et al., 2015) and visualized using FigTree Version - v1.4.4. For genome comparison, average nucleotide identity (ANI) was predicted using FastANI (Jain et al., 2018).

2.4. Microscopic observations of Microcoleus filaments

The morphology of *Microcoleus* filaments was documented from fresh material in stationary growth phase at day 40 of the experiment using an Olympus microscope BX41 and imaged with the attached Olympus SC30 digital camera (Olympus Imaging America). Morphological features including color, cell width, length, granulation, keritomization, level of constriction at cross-walls, attenuation of filaments, morphology of apical cells, and sheath characteristics were recorded.

2.5. Cell density and cell biovolume

Cell density and biovolumes were estimated from Lugol's preserved samples in triplicates, with the exception of a few strains/harvests grown in duplicates due to limited incubator space or incidental broken vials: *Microcoleus* sp. 1 ER6 (days 8 and 40) and ER12 (days 8, 13, 40, and 46), *M. anatoxicus* strains SR16, SR17, RC9, PTRS1 (days 40 and 46). *Microcoleus* sp. 1 ER6 was harvested on day 46 being grown as a singlet. Filaments were gently removed from the walls of the culture tubes using sterile disposable loops. Following modified methods from Harland et al. (2013) and Heath et al. (2014; 2016), the cultures were homogenized with the Ultra-Turrax probe (IKA Laboreknik, Germany), for at least 90 s or until mats were broken up into mostly solitary filaments and clumps less than 1 mm^3 as measured under the dissecting scope to ensure countable samples and random dispersal of the filaments. Between each sample, the probe was rinsed twice with Milli-Q water.

After homogenization, cultures were shaken to yield representative samples and 0.1 mL subsample was placed into a Palmer-Maloney counting chamber. The total length of all filaments observed in 30 random field of views was measured under 400x magnification for all replicates. Cell lengths and widths were measured for at least 30 cells and averaged for

each strain at each harvest date. To calculate the total cell biovolume for each sample, a series of equations were used as described below.

The average cell width (i.e., diameter) was used to estimate the total cell biovolume observed per sample using the equation for cylinder volume following the cell shape approximations by Hillebrand et al. (1999):

$$Biovolume = \frac{\pi}{4} * d^2 * h \quad (1)$$

where d = average cell diameter (μm) and h = total measured trichome length (μm). This calculated cell biovolume in μm^3 was used as value C in Eq. (2).

To calculate the total cell density and total cell biovolume for each sample, the following equation (Eq. (2)) from APHA (1992) was used:

$$Cell\ number\ or\ cell\ biovolume\ per\ mL = \frac{C * 1000\ mm^3}{A * D * F} \quad (2)$$

where C = total number of cells or biovolume of cells (μm^3) in analyzed area (30 fields of view); A = area of field of view calculated using the area of a circle, where the diameter of the field of view of the microscope used was 0.52 mm (total area equaling 0.21 mm^2), D = depth of field of view (0.40 mm), and F = number of fields of view analyzed (30).

2.6. Chlorophyll a analysis

Chlorophyll *a* (chl *a*) was measured fluorometrically using a Turner Designs Trilogy benchtop fluorometer with 7200–040 filter module (Turner Designs, San Jose, California) at George Mason University. The contents of each culture tube were filtered through a 0.45 μm membrane filter (Gelman GN-6) at a vacuum of 10 lbs/in for chl *a* and phaeopigment determination. During the final phases of filtration two drops of a 10 % $MgCO_3$ suspension were added to the filter to avoid premature acidification. The filters were placed in 20 mL plastic centrifuge vials and stored at −20 °C. Within 6 weeks of filtration, frozen filters were removed from the plastic vials and placed in a 15 mL ground glass homogenizer and 4 mL of dimethyl sulfoxide (DMSO) were added. The filter dissolved in the DMSO and the filter contents were ground for a minimum of 1 min moving the pestle up and down for full maceration. The contents of the homogenizer were rinsed with 90 % acetone into the 20 mL centrifuge tube and held at 4 °C overnight to complete the extraction. The following day the extracts were centrifuged for 10 min and the supernatant was transferred to a graduated cylinder and brought to a known volume. An aliquot of this extract was then placed in the fluorometer and chl *a* concentration was determined. Two drops of 6 M HCl were added to convert all chlorophyll to phaeopigment, and the fluorescence was again measured. The calibrated fluorometer was set to allow direct reading of chl *a* and phaeopigment concentrations in μg/L and these were proportioned back to μg/culture vial.

2.7. Toxin analysis

The glass tubes with 20 mL *Microcoleus* cultures were removed from the culture conditions and sent overnight on ice for toxin analysis to the State University of New York (SUNY-ESF) in Syracuse. Upon receipt at SUNY-ESF, *Microcoleus* filaments were gently scaped off the walls of the tubes with sterile disposable microbiological loops. The entire content of the tubes was filtered onto tared Whatman 934 AH glass fiber filters (nominal pore size 1.5 μm), dried by lyophilization, and reweighed. The filtrate was collected and analyzed for extracellular toxin content as described below. The dry weight mass retained by the filters was recorded and used as a measure of cell biomass.

The biomass retained on the filters was analyzed for particulate or intracellular toxins. The filters were extracted in 5 mL of 50 % acidified methanol containing 1 % acetic acid using a Branson 450 W probe sonicator equipped with a microtip for 1 min (three 20 second pulses) on ice. After sonication, the extract was clarified by centrifugation at 14,000 xg, and the filtrate passed through a 0.2 μm pore nylon filter prior to LC-MS/MS analysis. Prior studies using cyanobacterial cultures have shown that this protocol released greater than 90 % of microcystins, anatoxins, and PSP toxins from the cyanobacteria cells (Boyer, 2007). The filtrate was analyzed directly without further processing other than passage through a 0.2 μm nylon filter. All samples were analyzed for six anatoxins, anatoxin-a, homoanatoxin-a, and their respective α and β-dihydro epimers using EPA method 545 modified to include the additional congeners and two confirmation ions (Smith et al., 2020). Dihydroanatoxin-a was quantified against a secondary anatoxin-a standard, which in turn was quantified against an anatoxin-a certified reference standard obtained from NRC Canada. Given that α and β-dihydro epimers potentially interconvert (Méjean et al., 2016), the concentrations of the α and β-epimers were combined to give a single value. Due to the lack of certified reference standards, HTX and its respective dhHTX were quantified using the anatoxin-a standards. Chemical synthesis of dihydroanatoxin-a confirmed that the response factor for this toxin was similar to anatoxin-a and not a significant source of error. Spike experiments confirmed that ion suppression in these samples was <10 % and the thus final concentrations were not corrected for matrix effects. Method detection limits were calculated individually for all samples using the instrument detection limits at the time the same was run, the extract volume and the weight or volume of the sample extracted. Method detection limits for anatoxins (including the dihydro derivatives) were several orders of magnitude less than the measured concentrations and were generally less than 0.2 μg/g or 0.1 μg/L.

Once toxin concentrations (μg/g or μg/L) were gathered, we standardized the average total toxin concentration from each harvest to the respective average cell count data to be able to estimate intracellular and extracellular toxin quotas, as femtograms of toxin per cell (see Harland et al., 2013). Since toxin extraction results in the destruction of filaments, we assumed that the averaged values of each harvest would serve as a representative to the true values as within-strain starting inoculums do not have high variation (Brown, unpublished data).

2.8. Toxin degradation measurement

Microcoleus anatoxicus strains PTRS1 and SR16 grown for 49 days in duplicates were used to test the persistence of ATX and dhATX in our culture conditions, considering the fact that the monoclonal cyanobacterial cultures contain heterotrophic bacterial contaminants. After completing the toxin measurements as described above, the culture filtrate was filtered a second time through a Whatman 934 AH glass fiber filter, transferred to a new clean glass tube and placed near a west-facing window at lab room temperature. The toxin concentrations were measured every day to determine the toxin degradation rate. The aim of this experiment was to determine how long the cyanotoxins persisted in culture media in the presence of heterotrophic bacteria.

2.9. Statistical and graphical analyses

2.9.1. Variation of cell morphology across harvests—When estimating cell density and biomass, the average total cell length and widths specific for each harvest were applied as explained in Section 2.5. To determine whether to use harvest-specific cell size data in the data analyses or cell sizes averaged across the entire experiment for each strain, cell morphometries (lengths and widths) were analyzed to test whether they varied throughout the experiment for each strain. To analyze these differences in morphological characteristics through time, first the data were checked to determine if it met the assumptions of normality using a Shapiro-Wilk test. The data failed the normality test, therefore, we employed the Kruskal-Wallis test, a non-parametric test which compares differences in the median between three or more independent groups. A Dunnett's test with a Holm adjustment was used to detect post-hoc differences. These outcomes informed our decision to use harvest and strain-specific mean morphometric data in our biomass calculations (see Section 3.3 for more details).

2.9.2. Correlation between different cell density and cell biomass measures —To determine which measure, cell density or biovolume, was the most robust representative for growth rate analysis, they were quantified against chl *a* data. Chlorophyll *a* was used as it is the most representative of vital cells as it is a necessary molecule for living algal cells, although this measure also has hurdles (Schagerl et al., 2022). However, the data for cell biomass (cell density and biovolume) was taken at finer scale time intervals with more replicates, which would be more informative in analyzing the population growth models. Pearson's correlations were run between cell density and chl *a* concentration, and between cell biovolume and chl *a* concentration. The parameter with the highest correlation coefficient and significance with chl *a* (biovolume-Supplemental Fig. 3) were used.

2.9.3. Growth analyses—Based on measured cell growth in batch cultures, we estimated maximum growth rates defined as the rate the population increases in the absence of suppressing effects of density dependence on population growth (Perni et al., 2005) and time-specific growth rates within strains (Li et al., 2024). In this study, *Microcoleus* strains were grown in batch culture with initially non-limiting luxurious nutrient conditions in a controlled, laboratory setting. In batch culture, nutrient availability is highest during early stages of cell division and then decreases as the population grows and mats are formed

immobilizing the nutrients in the culture, which could influence the rate of strain growth rates throughout time. Comparing the maximum growth rates helps to remove the variability of nutrient-consumption and density-dependence through time.

2.9.3.1. Gompertz model.: To characterize the maximum growth rates of each strain, the biovolume data was fitted to a Gompertz model, a density-dependent population model (Blaszczak et al., 2023). The Gompertz model is a robust method for modeling microbial population growth and fits the data to a sigmoidal growth curve (Wang and Guo, 2024). The Gompertz model is log-linear model (Ives et al., 2003) and the overall growth curve of each strain can be described as

$$y_{i,t} = a_i + b_i * y_{i,t-1} \quad (4)$$

where $y_{i,t}$ is the natural log of the total biovolume (μm^3/mL) of strain(s) i on day t. a_i is the maximum growth rate, or the predicted growth rate when the density of the population is low, of strain i, and b_i is a parameter that describes the strength of density dependence.

Parameters in the Gompertz model were inferred in a Bayesian hierarchical framework. The underlying process model was

$$y_{i,t} \sim Normal(a_i + b_i * y_{i,t-1}, \sigma_p^2) \quad (5)$$

where $y_{i,t}$ is a latent-state representing the true natural log of the total biovolume density (μm^3/mL) of strain i on day t, and σ_p^2 is process error, or the variance of the data. The data were sampled using a Gaussian (normal) distribution. To account for observation error created by using multiple experimental replicates we used an observation model

$$Y_{r,i,t} \sim Normal(y_{i,t}, \sigma_o^2) \quad (6)$$

where $Y_{r,i,t}$ is the observed natural log of the total biovolume density (μm^3/mL) for replicate r of strain i on day t. This approach accounts for sample variability that is expected to occur among replicates because we did not subsample the same replicate each time, thus allowing us to separately estimate the underlying biological parameters of interest from sample variability.

The model was fit using the probabilistic programming language Stan (Carpenter et al., 2017), which generates a posterior probability distribution using Hamiltonian Monte Carlo (HMC), in the rstan package (Guo et al., 2016; Stan Development Team, 2024) in R (R Core Team, 2024). We ran 3 chains with 10,000 iterations for each chain.

2.9.3.2. Hypothesis testing and model comparison.: Five different models were produced using the methods described above (Section 2.9.3.1), where different combinations

of strains, based on different desired characteristics (i.e., anatoxin congeners, toxin concentrations produced, etc.) were grouped and data were fit to the Gompertz model (Table 2). Model 1 combined the biovolume data from all six strains ($i = 1$) and applied it to the model to produce one growth curve, generating one predicted maximum growth rate. Model 2 fit the biovolume data from each strain separately ($i = 1$ to 6) to the model, generating six different maximum growth rates. Model 3 grouped the data from non-toxic strains together (*Microcoleus* sp. strains ER6 & ER12) and all toxic strains together (*M. anatoxicus* strains SR16, SR17, RC9, and RR20), generating a predicted maximum growth rate for non-toxic strains and toxic strains ($i = 1$ to 2). Model 4 combined strains by their ability to produce different anatoxin congeners (e.g., non-toxic versus dhATX only versus ATX and dhATX producing strains), producing three predicted maximum growth rates ($i = 1$ to 3). Finally, model 5 analyzed strains clustered by the concentration of toxins during peak anatoxin production (non-toxic versus less toxic (<100 fg/cell) versus more toxic strains (>100 fg/cell) (see Fig. 4 for toxin concentrations). The best fit model was tested using the Watanabe-Akaike information criterion (WAIC). The model which produces the lowest WAIC values is considered the best fitting model and was used for analyzing how toxin-production can potentially affect *Microcoleus* growth. The posterior probability distribution of maximum growth rate was visualized using density plots in 'ggplot2' (Wickham, 2016).

2.9.3.3. Specific growth rate analysis.: To analyze specific growth rates for each harvest date, the following equation was employed:

$$\mu = \frac{ln(X_n) - ln(X_{n-1})}{T_n - T_{n-1}}$$

where ln is the function for taking the natural logarithm of a value, X_n= average biovolume ($\mu m^3\ mL^{-1}$) at time n (T_n) and X_{n-1}= average biovolume ($\mu m^3\ mL^{-1}$) at time n – 1 (T_{n-1}). Specific growth rates represent the change in the cell biovolume for a specific harvest, comparing cell biovolume of two consequent harvests. This measure is biologically indicative of step-wise growth in the population. Comparing peaks of toxin production to time-specific rates of growth can help promote further understanding of the energetic expenses of toxin production.

3. Results

3.1. Phylogenetic placement of Microcoleus strains

Single cyanobacterial MAGs with completeness > 95 % and contamination < 5 % were successfully retrieved from each *Microcoleus* strain. This phylogenetic tree illustrated the evolutionary relationships among the six *Microcoleus* strains under study (Fig. 2). *Microcoleus* taxa formed two clades – clade 1 which contained the anatoxin-producing species, and clade 2 was composed of non-toxic species (Fig. 2). Both non-toxic strains from the South Fork Eel River *Microcoleus* sp. 1 ER6 and ER12 belong to the same species as other non-toxic strains previously sequenced from Eel River (*Microcoleus* sp. strain PH2017 22 RUC O B) with shared average nucleotide (ANI) values of 99.37 % and 99.35 %, respectively (Supplemental Fig. 1). Toxic strains used in this study - SR16,

SR17, RC9 and PTRS1 (= *M. anatoxicus* type strain PTRS1) formed a cluster with another toxic *Microcoleus* strain (*Microcoleus* sp. strain 2_PH2015_08D_45_74) from the Eel River. All four strains studied here (e.g., SR16, SR17, RC9 and PTRS1 (= *M. anatoxicus* type strain PTRS1) shared over 99 % ANI and were assigned to *M. anatoxicus. Microcoleus* 2_PH2015_08D_45_74 from Eel River shared over 99 % ANI with *M. anatoxicus*. The *M. anatoxicus* cluster was sister to *Microcoleus* sp. CAWBG506 from New Zealand, sharing 94.38 % ANI to *M. anatoxicus* type strain PTRS1, but genetically distant from other toxic strains from New Zealand and Canada.

3.2. Variation of cell morphology across harvests and correlation between different biomass measures

In culture conditions, filament morphology greatly varied within each unialgal monoculture (see for details Supplemental Text 1). The filaments of *Microcoleus* sp. 1 were olive-green to light brownish with capitate apical cells with rounded or truncated calyptras (Fig. 3A–C). Cells were 5–9 μm wide and 0.63–7.5 μm long, slightly constricted at the cross walls. *Microcoleus anatoxicus* had olive-green to dark brown filaments, with some strains having a slight purple or orange hue (Fig. 3D–H). Cells were 5–9.3 μm wide and 2.5–6.7 μm long, typically not constricted, apical cell with wide rounded calyptras. Cell morphometrics varied through culture age, with shorter cells corresponding to the exponential phase.

The cell width of all strains varied ($H = 72.58–159.77$, $df = 9$ and $p < 0.05$ for all; Supplemental Table 2). The cell length of all strains varied significantly across each harvest ($H = 18.94–118.78$, $df = 9$ and $p < 0.05$ for all; Supplemental Table 3). Therefore, we used harvest-specific morphometric data in cell density and biovolume calculations rather than pooled-data. Shorter cell lengths corresponded with the exponential growth phase (days 0–29), which could be indicative of more rapid replication. Cell biovolume and chl *a* had a stronger correlation ($r = 0.55$, $p = 0.0006$) than did cell density with chl *a* ($r = 0.44$, $p = 0.0066$) leading to biovolume being used as a measure of biomass over cell density (Supplemental Fig. 3).

3.3. Toxin production

All *Microcoleus anatoxicus* strains continuously produced detectable dhATXs and two strains (SR16 and SR17) also produced detectable ATX during the entire experiment (Fig. 4). The timing of peak toxin production varied for each strain but occurred during the exponential growth phase. For strains SR16 and SR17, peak ATX concentrations occurred at days 19 and 13 and peak dhATXs concentrations occurred at days 26 and 13, respectively (Fig. 4A, B). Both strains produced higher total concentrations of ATX than of dhATXs. Strain SR16 produced maximum 314 fg/cell total ATX and 186 fg/cell total dhATXs, which is a much higher concentration of toxins than strain SR17 (maximum 60 fg/cell total ATX and 5 fg/cell total dhATXs). The maximum total dhATXs concentrations for strain RC9 occurred at day 13 (Fig. 4C) and for strain PTRS1 at day 26 (Fig. 4D). Strain PTRS1 produced more total dhATXs than RC9, with maximum concentrations being 195 fg/cell while the maximum concentration of *M. anatoxicus* strain RC9 was 25 fg/cell. Strains SR16 and PTRS1 will be hereafter referred to as more toxic strains (producing >100 fg/cell of total

toxins during peak concentrations), while strains SR17 and RC9 (producing <100 fg/cell of total toxins during peak concentrations) will be referred to as the less toxic strains.

For strain SR16, the majority of the ATX quota was extracellular (37–73 %) as well as for dhATXs (98–100%) (Fig. 5A). In contrast, in strain SR17 most toxins were intracellular (e.g., intracellular ATX ranging from 88.95 to 100 % and dhATXs 91–100 %, Fig. 5B). Similarly, the dhATXs produced by strain RC9 was predominantly intracellular (47–100 %, Fig. 5C), while the dhATXs from PTRS1 was mostly extracellular (64–92 %, Fig. 5D).

There was less variation in intracellular toxin concentrations among strains compared to total toxin concentrations (Fig. 5). Strain SR16 had a maximum intracellular ATX concentration of 1.50 fg/cell which is only about two times higher than SR17 (0.74 fg/cell) and a maximum intracellular dhATXs concentration of 0.07 fg/cell which is only about 2.5 times higher than SR17 (0.03 fg/cell). Strain PTRS1 peaked at 1.02 fg/cell which is actually slightly lower than strain RC9 (1.12 fg/cell).

In summary, *M. anatoxicus* strains SR16 and PTRS1 produced at least five-fold higher total maximum toxin concentrations compared to their less toxic counterparts. The toxins in strains SR16 and PTRS1 were predominantly extracellular with maximum concentrations recorded 6 to 13 days after the peak toxin production in the other two less toxic strains.

3.4. Toxin degradation

Microcoleus-free culture liquid containing anatoxins stored in an air-conditioned laboratory under ambient light showed degradation of both ATX and dhATXs in six days (Fig. 6). The extracellular dhATXs concentrations of *M. anatoxicus* strain PTRS1 dropped its average toxin concentration from 166 μg/L to nearly 0 after six days (Fig. 6b). This strain did not produce detectable ATX. *Microcoleus anatoxicus* strain SR16 from the Scott River which produced both toxins showed the same rate of toxin degradation over six days for ATX concentrations of 37 μg/L and dhATXs of 78 μg/L (Fig. 6a).

3.5. Microcoleus growth curves and Gompertz model

All six *Microcoleus* strains grew well in BG11 and formed visible mats on the water surface or dense filament agglomerates after 30 days in culture, which indicated the end of the exponential phase and a stagnation of biomass accrual (Figs. 7 and 8). The Gompertz model fit the biovolume data well for all models run (all $\widehat{R}$ values ≤1.05, Supplemental Table 5). Out of all growth models run, model 5 returned the lowest WAIC value followed by models 1, 3, 4, and 2 (Table 3). The models return different predicted maximum growth rates (Supplemental Table 5) for each grouping of strains (Supplemental Table 4). When running model 2, all strains were independently fit to the data. The output of model 2 show that *M. anatoxicus* strains SR16 and PTRS1 have the highest predicted maximum growth rates, whereas for all non-toxic and less toxic strains, the values are similar. The output of model 5 further supports this finding, with the more toxic strains having the fastest predicted maximum growth rates (Table 4). Despite model 2 not returning the best fit, we used it here to illustrate the individual variation in predicted maximum growth rates (Fig. 9A), whereas model 5 was used to provide statistical evidence that the more toxic strains achieve higher

maximum growth rates than did non-toxic and less toxic *Microcoleus* strains in this study (Fig. 9B).

3.6. Specific growth rates

Patterns of specific growth rates were compared to the timeline of toxin production to elucidate energetic responses with toxin production (Fig. 10). For non-toxic strains (*Microcoleus* sp.1 ER6 and ER12), specific growth rates ranged from −0.02 to 0.26, with the lowest rate with negative growth at day 40 (during the stationary phase) and the highest growth occurring at day 8 (Fig. 10A). For less toxic strains (*M. anatoxicus* strain SR17 and RC9), specific growth rates ranged from −0.02 to 0.28, with the lowest growth rate occurring during the stationary phase (days 40 and 46) and the highest growth rate occurring on day 15. However, the lowest specific growth rates occurring during the exponential phase occurred on days 13 (0.13) and 26 (0.11), with day 13 coinciding with anatoxin production (Fig. 10B). Specific growth rates were all much lower for the stationary phase. For more toxic strains (*M. anatoxicus* strains SR16 and PTRS1), specific growth rates ranged from −0.02 to 0.32, with the fastest specific growth rate occurring on day 15. Days 19 and 26 were when strains experienced maximum anatoxin concentrations, which is also corresponded with depressions of growth rates (0.14 and 0.11, respectively) (Fig. 10C).

4. Discussion

Toxic and non-toxic strains or genotypes of *Microcoleus* are commonly reported in stream watersheds globally (Wood et al., 2018; Bouma-Gregson et al., 2019; Valadez-Cano et al., 2023), but their species identity remains poorly known. Cyanobacterial and algal species belonging to the same genus are adapted to different environmental conditions which require species-level identification to obtain the most precise information about their responses to environmental stressors (Stevenson and Bahls, 1999). This study extended the known range of a potent anatoxin-producing species, i.e., *Microcoleus anatoxicus,* from major coastal stream watersheds in northern California – Russian, Eel and Klamath Rivers to the inland Rock Creek in the Southern Cascade Mountain Range. Outside of North America, *M. anatoxicus* has been genetically confirmed to proliferate in the river Areuse in Switzerland (Junier et al., 2024). This species is genetically distant from other ATX producing *Microcoleus* species from flowing waters in Canada and New Zealand (Wood et al., 2018; Valadez-Cano et al., 2023).

In field and laboratory studies, *Microcoleus* has shown to have wide nitrogen tolerances, preferring slightly elevated but still low levels of nitrogen (Wood et al., 2017), with much of the research being done on *M. autumnalis* and other strains (Heath et al., 2014; 2016). Currently, little information has been gathered on the species-specific responses of *M. anatoxicus*. Stancheva et al. (2024) elucidated that growth of *M. anatoxicus* might be slightly stimulated by increased salinity with no effects on toxin production, and can persist long-term with no external sources of nitrogen. Additionally, in the South Fork Eel River (Finlay et al., 2011; Weigel et al., 2020) and Russian River, strains co-existed with N_2-fixing algae while in the Scott River and Rock Creek, no N_2-fixing algae were noted (Stancheva, personal observations). Whether or not nitrogen fixation by N_2-fixing

cyanobacteria can serve as a potential nitrogen source to *Microcoleus* remains unknown. Our results highlighted that the more toxic *M. anatoxicus* strains can achieve faster growth rates under high nutrient laboratory conditions, which may explain why toxic strains tend to be reported in California watersheds with more elevated dissolved inorganic nitrogen than sites where non-toxic strains were identified (Bouma-Gregson et al., 2019). This study aims to explore the ecophysiological and toxin responses from *M. anatoxicus* with no nutrient limitations.

4.1. Microcoleus strain identity

Microcoleus strain morphology and molecular profiles were investigated here and compared to others to understand the global distribution of different *Microcoleus* species. The non-toxic *Microcoleus* strains ER6 and ER12 belonged to the same species as the other non-toxic *Microcoleus* genotypes previously detected in the Eel and Russian Rivers (Bouma-Gregson et al., 2019), indicating their potentially widespread distribution in northern California. The species identity of this strain needs further taxonomic investigations and formal description if novel to science. All toxic strains in this study were phylogenetically identified to belong to *Microcoleus anatoxicus,* which expands its known area of distribution to several watersheds in northern California, including Eel River where it was previously recorded as *Microcoleus* 2_PH2015_08D_45_74 by Bouma-Gregson et al. (2019; 2021). Our more detailed MAG comparison rooted on 120 core genes, compared to 29 core genes used by Valadez-Cano et al. (2023) confirmed their results that the toxic *Microcoleus* strains from Canada are more closely related to strains from New Zealand than to Californian strains, despite the closer geographical distance of California and Canada. Junier et al. (2024) reported toxic *Microcoleus* strain NeuA isolated from Switzerland sharing 96.04% Average Nucleotide Identity (ANI) with *M. anatoxicus* type strain PTRS2, highlighting their close relationship. The second-most closely related toxigenic strain from New Zealand, *Microcoleus* strain CAWBG506 (Tee et al., 2021) still represents a different species with 94% shared ANI to *M. anatoxicus* type strain PTRS1. Whether *M. anatoxicus* is an endemic or cosmopolitan species is a topic which is currently growing and warrants further investigations. Indeed, Californian algal flora is characterized by a high endemism and some diversity hot-spots (Bahls, 2024; Mora et al., 2024).

In terms of mat and filament morphology in culture conditions, we observed great variation in the four toxic strains. Cell length, width, granulation, pseudovacuolation, apical cell shape and mat characteristics vary with age and withing different areas of the mats. The strains also vary in color hue to a certain degree based on the age of cultures, likely due to factors such as chromatic adaptation and the ability of cyanobacteria to alter their phycobiliproteins based on environmental factors (Kehoe, 2010). However, the brownish toxic and olive-greenish non-toxic strains studied here generally kept their characteristic color in culture conditions, probably due to species-specific combination of phycoerythrin and phycocyanin (Komárek and Anagnostidis, 2005). Additionally, the strains studied here exhibited variations in mat gross morphology and growth rates, with some strains exhibiting tychoplanktonic growth forms. These atypical and differential growth forms may complicate mitigations efforts. This research further supports that *Microcoleus* species differentiation

requires a polyphasic approach, linking together molecular, morphological, and ecological data (Hašler et al., 2012).

4.2. Toxin production and its implications

Microcoleus anatoxicus exhibited strain-dependent variation in ATX congeners and concentrations produced, similarly to other *Microcoleus* species such as *M. autumnalis* (Heath et al., 2010). Within this study, the timing of toxin-production varied between strains as well. Previous research suggested that mat toxin concentrations can be predicted from the relative abundance of toxigenic genotypes (Heath et al., 2010; Kelly et al., 2018, 2019). Our experimental results provide further supporting evidence that different strains of the same toxigenic species can peak anatoxin concentrations at different times in their life history (see Harland et al., 2013; Heath et al., 2014; 2016; Wood et al., 2017). *Microcoleus* filaments may colonize and form mats in different stream reaches at differing times, further promoting high variability of concentrations or the persistence of anatoxins in the field.

In strains producing ATX and dhATXs from Klamath River watershed (i.e., *M. anatoxicus* strains SR16 and SR17), higher concentrations of ATX were recorded than dhATXs, which is mirrored in field studies from Eel and Russian Rivers (Kelly et al., 2019). In contrast, the three strains of *M. anatoxicus* isolated from Russian River in 2015, produced 300 times more dhATX than ATX during the first three years in culture conditions (Conklin et al., 2020; Stancheva et al., 2024). Recent experiments with *M. anatoxicus* strain PTRS1 has not detected ATX (Stancheva et al., 2024, this study), but only dhATXs, which leaves the question if it completely lost the ability to produce ATX through a modification of the ATX pathway (Méjean et al., 2016) or cellular conditions promoted expression of the *anaK* gene, encoding the putative F420 dependent oxidoreductase which converts ATX to dhATX (Kust et al., 2020). This is a relatively underexplored area and warrants further transcriptomic investigations. There are numerous reports of cyanobacteria losing the ability to produce all toxins when stored long-term in culture (Park et al., 1993; Gallon et al., 1994; Rantala-Ylinen et al., 2011). This is generally thought to be due to the loss of the biosynthetic operon under the luxurious growth conditions used for culturing. For example, Jiang et al. (2015) reported that loss of the ability to produce anatoxins may be caused by a deletion of genes within the anatoxin gene cluster. However, there are few reports of loss of a specific congener while retaining the parent biosynthetic pathway. Whether or not there is a physiological advantage to producing one or multiple anatoxins depends on the currently unknown function and benefit of these toxins in the host organism. Molecular analyses in progress will bring more information on this shift from producing two detectable anatoxin congeners to only one.

More toxic *M. anatoxicus* strains SR16 and PTRS1 had higher percentage of extracellular toxin concentrations, indicative of passive or active transportation of toxins across cell membranes. It is known that shipping or other mechanical stress can cause cells to lyse and release toxins. Despite strains being shipped for toxin analysis together during the same time and by the same method for each harvest, a vastly different ratio of extracellular to intracellular toxins emerged. Like the cyanobacterial toxin microcystin, where a putative transporter has been identified as part of the mcy operon (*mcyH*; Christiansen et al., 2003),

the *anaI* gene has been identified as a putative transporter in *Oscillatoria* PCC 6506 and *Cylindrospermum stagnale* PCC 7417 (Mejean, 2016). Kust et al. (2020) suggests that anatoxins are transported through cell membranes, which our findings support. Conklin et al. (2020) reports the *anaI* gene present in *Microcoleus anatoxicus* strain PTRS3, which could serve as evidence of our more toxic strains transporting anatoxins extracellularly. However, to answer this question, targeted studies need to be designed and conducted.

Strains which had higher levels of extracellular anatoxins showed morphology indicative of unhealthy filaments, such as reddish rather than brown-olive green color and cells with ruptured walls (Fig. 3D, F), possibly related to leaking of toxins. Sinha et al. (2014) reported that the production of cylindrospermopsin in *Cylindrospermopsis raciborskii* (now *Raphidiopsis racoborskii* (Wołoszyńska) Aguilera et al. is likely related to stress and adaptation responses. It is unclear whether anatoxin production is also related to stress responses but the physiological health of the more toxic *M. anatoxicus* strains could provide evidence of stressed cells. Stancheva et al. (2024) used one of the strains with high production of toxins (i.e., strain PTRS1) in previous experiments and recorded similar cell wall damage (Stancheva et al., 2024) which indicates that this feature may be strain specific. The mechanisms contributing to poor filament health in some strains could be of ecological importance, as high levels of extracellular anatoxin concentrations in the field could be contributed from unhealthy cells with lysed or broken cell walls. Anatoxin-a could also be produced as a defense mechanism when *Microcoleus* cells are early in mat development, especially for unhealthy filaments. Extracts from *M. anatoxicus* containing anatoxins have been shown to be lethal to macroinvertebrates (Anderson et al., 2018), although the toxicity could be magnified by other unknown compounds as suggested by Kelly et al. (2020). Similarly, Toporowska et al. (2014) reported that the crude extract from ATX-producing *Dolichospermum* species was more toxic to benthic *Chironomus* larvae than the pure anatoxins, highlighting the potential other metabolites could contribute to poisoning of benthic organisms. Quiblier et al. (2013) also discusses that more terrestrial organisms have been implicated by cyanotoxin poisonings than aquatic species. Anatoxins have been proven to be lethal to many vertebrates such as the rainbow trout (*Oncorhynchus mykiss*), mallard duck (*Ana platyrhyncos*) and ring-neck pheasant (*Phasianus colchicus*), and many mammals (Plata-Calzado et al., 2022 and references therein). Whether toxicity to higher level organisms evolved spuriously or is the main biological function of anatoxins is still under debate (Holland and Kinnear, 2013; Plata-Calzado et al., 2022 and references therein). However, the public safety (USEPA, 2015; WHO, 2020) and ecological issues surrounding the presence of anatoxins in aquatic systems is evident.

4.3. Toxin degradation

Our lab experiments showed that the extracellular toxin concentrations were much higher than the intracellular toxin concentrations in the two more toxic *M. anatoxicus* strains. It was unknown prior to running the toxin degradation experiment, whether the toxins persisted long-term in culture media or consistently leaked from the cells. We hypothesized that the high extracellular fraction of anatoxin congeners was due to cell lysis (Testai, 2021) and that the toxins were consistently being released from stressed filaments. Culturing conditions and the total biomass of mats within the cultures could have influenced the release of anatoxins

to the extracellular fraction as well. The development of additional mucilaginous layers around the *Microcoleus* trichomes could stabilize the cells and increase the retention of anatoxin in the intracellular fraction (Stancheva et al., 2024).

The complete degradation of the extracellular ATX and dhATX remaining in *Microcoleus*-free culture media required approximately six days in ambient day-light lab conditions with constant temperature around 20 °C. This provided evidence for the consistent leaking of toxins as harvests occurred within 2–7 days to each other, whereas there was a consistent report of extracellular toxins throughout the experiment. The degradation of anatoxins in the media could have been due to biological or chemical processes. Yang (2007) reported a first-order half-life for anatoxin-a of 4–10 h in natural light under elevated pH conditions. Degradation of anatoxin-a is dependent on the light intensity and pH, with higher pH favoring degradation reactions (Stevens and Krieger, 1991; Yang, 2007). These laboratory experiments may or may not reflect what happens under natural conditions. Smith and Sutton (1993) in laboratory experiments with a sediment microbial community from a reservoir reported a five-day half-life for anatoxin-a, with toxins persisting for at least 21 days at pH 4, and maintaining detectable levels after 14 days at pH 8 and 10. As the chemical degradation of anatoxin-a is a photochemical reaction, sediment resuspension in these experiments may have shaded the toxins for photolysis. However, biodegradation of anatoxins is also mediated by heterotrophic microorganisms, such as the aerobic rod bacterium *Pseudomonas* (Kormas et al., 2013). The *Microcoleus* culture liquid tested for ATX degradation was deliberately not axenic and contained rod-shaped bacteria. The role these bacteria might play in anatoxin biodegradation is unknown.

4.4. Microcoleus Growth

All six *Microcoleus* strains showed similar growth with mat formation around day 30 after inoculation with growth being slowed by density-dependence. The formation of the mats differed morphologically across strains, both in the filament color hue and the propensity to attach to the culture walls (Supplemental Fig. 2). These features cannot be quantified but may be important in providing diverse strategies for occupying different substrate types in the environment with favorable microhabitat conditions.

We detected differences in the specific growth rates, which declined more or less steadily along the lifecycle of non-toxic strains. In toxigenic strains, the rate of growth is more variable with strong declines coinciding with the day of maximum toxin production, indicative for the high energetic cost of this process. Furthermore, the pulse of high toxin concentrations may trigger a synergetic response by the culture microbiome, which may also affect *Microcoleus* growth. Two or three days later the filament growth rate rebounded strongly (Fig. 10). Despite this, the maximum growth rate model (Model 5) which best fit the data showed that more toxic strains (*M. anatoxicus* strains SR16 and PTRS1) have overall higher maximum growth rates than less toxic (*M. anatoxicus* strains SR17 and RC9), and non-toxic strains (*Microcoleus* sp. 1 strains ER6 and ER12) when grown in the same laboratory-controlled conditions.

Our results contrast with Heath et al. (2016), where non-toxic *Phormidium* (presumably *Microcoleus*) strains had faster maximum growth rates than toxic strains across different

nitrogen and phosphorus concentrations, with their results highlighting the effect of nutrient concentrations on growth and toxin production. Differences between our study design and Heath et al. (2016) could contribute to this differential result. Concentrations of nitrate and phosphate used by Heath et al. (2016) ranged from 0.3 to 1.5 mM and 0.0008–0.1 mM, respectively, and were much lower than the concentrations used in our study (e.g., BG11 medium with 17.6 mM of nitrates and 0.22 mM of phosphates (UTEX Culture Collection of Algae, Austin, TX, USA). In our study, strains were grown with no limiting nutrients so that the effects of toxin production could be analyzed without the potential confounds of nitrogen and phosphorus metabolism mitigating growth and toxin production. Additionally, New Zealand strains were grown under lower light irradiance of 36 μmoles/m^2/s (Heath et al., 2016), compared to our experiment using irradiance of 100 μmoles/m^2/s. Furthermore, Valadez et al. (2023) and our phylogenetic results support that the strains from New Zealand likely belong to a different species than *Microcoleus anatoxicus.* Our data should not be generalized across all toxic and non-toxic *Microcoleus* species as different cyanobacterial species have species-specific physiology, growth optima and environmental tolerances. We suggest that taking a species-level approach when working with *Microcoleus* is important as it may be a major differentiating factor between our results and those from Heath et al. (2016) and could provide valuable information for understanding factors contributing to *Microcoleus* blooms in different regions globally.

When translating laboratory outcomes to environmental applications, we should consider that experimental batch culture conditions differ from the environment by lower light, decreasing nutrient availability over time and lack of water velocity leading to accumulation of toxic compounds around the mats during the stationary growth phase. However, the main environmentally applicable conclusion from laboratory experiments with different *Microcoleus* strains (Heath et al., 2014; 2016, this study) is that the cells produce much more toxins during the exponential growth phase and early stages of mat formation, which could be related to defense mechanisms or quorum sensing of population density (Miller and Bassler, 2001). Once the mats are established and grow in thickness, their toxin quota decrease, but other harmful compounds may be excreted (Andersen et al., 2018), suggesting that *Microcoleus* mats could be harmful even when anatoxin concentrations are low. The total toxin concentrations produced by *Microcoleus* mats in the environment depend on the cell density and toxin quota. Large cyanobacterial field biomass with low toxin quota, may pose a lower public-health concern (nuisance vs. harmful bloom) compared to smaller mats under stressful conditions which increase the toxin quota (Horst et al., 2014; Stancheva et al., 2024). Therefore, understanding factors that contribute to variation in toxin quota is important to recognize the impacts of cyanobacterial HABs, and lab manipulative experiments are helpful research tool despite some shortcomings.

5. Conclusion

The growth and toxin production of two different *Microcoleus* species from northern California were assessed, represented by six different strains. Both species are widespread throughout northern California watersheds, highlighting the importance to understand their growth rate responses and potential toxin-production. Toxin production was thought to be an energetically expensive process, as evidenced by slowed specific growth rates during

the time of maximum toxin production. Despite this, the more toxic *M. anatoxicus* strains were able to achieve faster predicted maximum growth rates and produced higher fractions of extracellular anatoxins. In the absence of nutrient limitations, the energetic expense of toxin production did not yield slower maximum growth rates in more toxic *M. anatoxicus*, which could highlight the importance of nutrients in modulating its production. Additionally, high concentration of extracellular anatoxins is of ecological concern and identifying factors contributing to this transport of toxins is important. Lower physiological health of more toxic strains of *M. anatoxicus* could represent a trade-off between high toxin production, rapid growth, and physiological integrity. The mechanism for toxin transport outside of cells is still unknown but a plausible explanation in this study is the leaking or transport of toxins through damaged cell walls. The intraspecific variation in growth and toxin production in *M. anatoxicus* strains highlights the need for transcriptomic studies to identify differential genetic responses. Additionally, more laboratory-based studies are needed to identify environmental variables at ecologically relevant conditions contributing to variations in cellular growth and physiological responses. Furthermore, the patterns expected based on the laboratory and transcriptomic evidence need to be linked back to field studies for confirmation. The rates of growth and the concentrations of toxins produced by *Microcoleus* have important implications for public safety, risk assessment, and ecological health. Toxigenic strains which achieve rapid growth and high levels of toxin production may elicit more animal poisoning events. This study provides ecophysiological information on the growth and toxin-production variation among strains of *M. anatoxicus* which may be beneficial for the management and mitigation of benthic harmful cyanobacterial blooms in running waters.

Supplementary Material

Refer to Web version on PubMed Central for supplementary material.

Acknowledgements

Authors are thankful to three anonymous reviewers who provided valuable comments and suggestion which improved the quality of the publication. We thank Marco Sigala, Cajun James, Laurel Genzoli, Bonnie Bennett, Joshua Cahill for providing field samples for isolation of *Microcoleus*, and Emma Boyden and Laura Birsa for the laboratory research support at George Mason University. This work was supported by the US National Science Foundation (Grant number NSF-URoL:EN: 2222322) to Ramesh Goel (PI) and Rosalina Stancheva, Joanna Blaszczak, and Robert Shriver (Co-PIs), and PhD students Sydney M. Brown and Abeer Sohrab, NSF Division of Environmental Biology (Grant number 2042915 to PI Blaszczak) which supported Jordan Zabrecky, NIEHS (1P01ES028939-01) and NSF (OCE-1840715) through the Great Lakes Center for Fresh Waters and Human Health at Bowling Green State University to Gregory Boyer for toxin measurements.

Data availability

Data will be made available on request.

References

Abarka N, Stancheva R, Skibbe O, Schimani K, Kusber W-H, Zimmermann J, Jahn R, 2023. Gomphadelpha (Bacillariophyceae) – a new genus name for taxa formerly subsumed within the name *Gomphoneis herculeanum*-complex. Nova Hedwig. 117, 213–254. 10.1127/nova_hedwigia/2023/0859.

Amorim CA, Moura AN, 2021. Ecological impacts of freshwater algal blooms on water quality, plankton biodiversity, structure, and ecosystem functioning. Sci. Total Env. 758, 143605. 10.1016/j.scitotenv.2020.143605. [PubMed: 33248793]

Andrews S, 2010. FastQC: A Quality Control Tool for High Throughput Sequence Data [Online]. Available online at: http://www.bioinformatics.babraham.ac.uk/projects/fastqc/.

Anderson B, Voorhees J, Phillips B, Fadness R, Stancheva R, Nichols J, Orr D, Wood SA, 2018. Extracts from benthic anatoxin-producing *Phormidium* are toxic to 3 macroinvertebrate taxa at environmentally relevant concentrations. Environ. Toxicol. Chem. 37 (11), 2851–2859. 10.1002/etc.4243. [PubMed: 30066467]

American Public Health Association (APHA), 1992. Standard Methods For the Examination of Water and Wastewater. American Public Health Association (APHA), Washington, DC, USA.

Bahls L, 2024. Plate tectonics, long-distance dispersals and chance introductions can explain many trans-pacific disjunctions. Diatom. Res. 10.1080/0269249X.2024.2383679.

Blaszczak JR, Yackulick CB, Shriver RK, Hall RO Jr., 2023. Models of underlying autotrophic biomass dynamics fit to daily river ecosystem productivity estimates improve understanding of ecosystem disturbance and resilience. Ecol. Lett. 26, 1510–1522. 10.1111/ele.14269. [PubMed: 37353910]

Bolger AM, Lohse M, Usadel B, 2014. Trimmomatic: a flexible trimmer for illumina sequence data. Bioinform. 30 (15), 2114–2120. 10.1093/bioinformatics/btu170.

Bouma-Gregson K, Kudela RM, Power ME, 2018. Widespread anatoxin-a detection in benthic cyanobacterial mats throughout a river network. PLoS. One. 13 (5), e0197669. 10.1371/journal.pone.0197669. [PubMed: 29775481]

Bouma-Gregson K, Olm MR, Probst AJ, Anantharaman K, Power ME, Banfield JF, 2019. Impacts of microbial assemblage and environmental conditions on the distribution of anatoxin-a producing cyanobacteria within a river network. ISME J. 13, 1618–1634. 10.1038/s41396-019-0374-3. [PubMed: 30809011]

Bouma-Gregson K, Crits-Christoph A, Olm MR, Power ME, Banfield JF, 2021. Microcoleus (Cyanobacteria) form watershed-wide populations without strong gradients in population structure. Mol. Ecol. 31 (1), 86–103. 10.1111/mec.16208. [PubMed: 34608694]

Boyer GL, 2007. The occurrence of cyanobacterial toxins in New York lakes: lessons from the MERHAB-lower great lakes program. Lake Reserv. Manag. 23, 153–160. 10.1080/07438140709353918.

Carpenter B, Gelman A, Hoffman MD, Lee D, Goodrich B, Betancourt M, et al. , 2017. Stan: a probabilistic programming language. J. Stat. Softw. 76 (1), 1–32. [PubMed: 36568334]

Conklin KY, Stancheva R, Otten TG, Fadness R, Boyer GL, Read B, Zhang X, Sheath RG, 2020. Molecular and morphological characterization of a novel dihydroanatoxin-a producing *Microcoleus* species from the Russian river, California, USA. Harmful. Algae. 93, 101767. 10.1016/j.hal.2020.101767. [PubMed: 32307065]

Chaumei PA, Mussig AJ, Hugenholtz P, Parks DH, 2020. GTDB-Tk: a toolkit to classify genomes with the genome taxonomy database. Bioinform. 36 (6), 1925–1927. 10.1093/bioinformatics/btz848.

Christiansen G, Fastner J, Erhard M, Börner T, Dittmann E, 2003. Microcystin biosynthesis in Planktothrix: genes, evolution and manipulation. Microbiol. (N. Y) 185, 564–572. 10.1128/JB.185.2.564.

Finlay JC, Hood JM, Limm MP, Power ME, Schade JD, Welter JR, 2011. Light-mediated thresholds in stream-water nutrient composition in a river network. Ecol. 92, 140–150. 10.1890/09-2243.1.

Gallon JR, Kittakoop P, Brown EG, 1994. Biosynthesis of anatoxin-a by *Anabaena flos-aquae*: examination of primary enzymic steps. Phytochem. 35 (5), 1195–1203. 10.1016/S0031-9422(00)94821-0.

Genzoli L, Hall RO Jr, Otten TG, Johnson GS, Blaszczak JR, Kann J, 2024. Benthic cyanobacteria proliferations drive anatoxin production throughout the Klamath river watershed, California, USA. Freshw. Sci. 00 (3), 00. −00. https://www.journals.uchicago.edu/doi/10.1086/731975.

Gugger M, Lenoir S, Berger C, Ledreux A, Druart J, Humbert J, Guette C, Bernard C, 2005. First report in a river in France of the benthic cyanobacterium *Phormidium favosum*

producing anatoxin-a associated with dog neurotoxicosis. Toxicon. 45 (7), 919–928. 10.1016/j.toxicon.2005.02.031. [PubMed: 15904687]

Guo J, Goodrich B, Gabry J Package 'rstan'. In: R package version 2.11.1. 2016.

Hamill KD, 2001. Toxicity in benthic freshwater cyanobacteria (blue-green algae): first observations in New Zealand. N. Z. J. Mar. Freshwater Res. 35, 105–1059. 10.1080/00288330.2001.9517062.

Harland FMJ, Wood SA, Moltchanova E, Williams WM, Gaw S, 2013. *Phormidium autumnale* growth and anatoxin-a production under iron and copper stress. Toxins (Basel) 5, 2504–2521. 10.3390/toxins5122504. [PubMed: 24351714]

Hašler P, Dvorák P, Johansen JR, Kitner M, Ondrej V, Poulíčková A, 2012. Morphological and molecular study of epipelic filamentous genera Phormidium, Microcoleus and Geitlerinema (Oscillatoriales, Cyanophyta/Cyanobacteria). Fottea. 12 (2), 341–356. 10.5507/fot.2012.024.

Heath MW, Wood SA, Ryan KG, 2010. Polyphasic assessment of fresh-water benthic mat-forming cyanobacteria isolated from New Zealand. FEMS. Microbiol. Ecol. 73, 95–109. 10.1111/j.1574-6941.2010.00867.x. [PubMed: 20455945]

Heath MW, Wood SA, Barbieri RF, Young RG, Ryan KG, 2014. Effects of nitrogen and phosphorus on anatoxin-a, homoanatoxin-a, dihydroanatoxin-a and dihydrohomoanatoxin-a production by *Phormidium autumnale*. Toxicon. 92, 179–185. 10.1016/j.toxicon.2014.10.014. [PubMed: 25449104]

Heath M, Wood SA, Young RG, Ryan KG, 2016. The role of nitrogen and phosphorus in regulating Phormidium sp. (cyanobacteria) growth and anatoxin production. FEMS. Microbiol. Ecol. 92, fiw021. 10.1093/femsec/fiw021. [PubMed: 26862139]

Hillebrand H, Dürselen C, Kirschtel D, Pollingher U, Zohary T, 1999. Biovolume calculation for pelagic and benthic microalgae. J. Phycol. 35 (2), 403–424. 10.1046/j.1529-8817.1999.3520403.x.

Holland A, Kinnear S, 2013. Interpreting the possible ecological role(s) of cyanotoxins: compounds for competitive advantage and/or physiological aide? Mar. Drugs. 11, 2239–2259. 10.3390/md11072239. [PubMed: 23807545]

Horst GP, Sarnelle O, White JD, Hamilton SK, Kaul RB, Bressie JD, 2014. Nitrogen availability increases the toxin quota of a harmful cyanobacterium, *Microcystis aeruginosa*. Water. Res. 54, 188–198. 10.1016/j.watres.2014.01.063. [PubMed: 24568788]

Huisman J, Codd GA, Paerl HW, Ibelings BW, Verspagen JMH, Visser PM, 2018. Cyanobacterial blooms. Nat. Rev. Microbiol. 16, 471–483. 10.1038/s41579-018-0040-1. [PubMed: 29946124]

Ives AR, Dennis B, Cottingham KL, Carpenter SR, 2003. Estimating community stability and ecological interaction from time-series data. Ecol. Monogr. 73 (2), 301–330. 10.1890/0012-9615(2003)073[0301:ECSAEI]2.0.CO;2.

Jain C, Rodriguez-R LM, Phillippy AM, Konstantinidis KT, Aluru S, 2018. High throughput ANI analysis of 90K prokaryotic genomes reveals clear species boundaries. Nat. Commun. 9, 5114. 10.1038/s41467-018-07641. [PubMed: 30504855]

Jiang Y, Song G, Pan Q, Yang Y, Li R, 2015. Identification of genes for anatoxin-a biosynthesis in *Cuspidothrix issatschenkoi*. Harmful. Algae. 46, 43–48. 10.1016/j.hal.2015.05.005.

Johnston LH, Huang Y, Bermarija TD, Rafuse C, Zamlynny L, Bruce MR, Graham C, Comeau AM, Valadez-Cano C, Lawrence JE, Beach DG, Jamieson RC, 2024. Proliferation and anatoxin production of benthic cyanobacteria associated with canine mortalities along a stream-lake continuum. Sci. Total. Environ. 917, 170476. 10.1016/j.scitotenv.2024.170476. [PubMed: 38290679]

Junier P, Cailleau G, Fatton M, Udriet P, Hashmi I, Bregnard D, Corona-Ramirez A, di Francesco E, Kuhn T, Mangia N, Zhioua S, Hunkeler D, Bindschedler S, Sieber S, Gonzalez D, 2024. A cohesive *Microcoleus* strain cluster causes benthic cyanotoxic blooms in rivers worldwide. Water. Res. X. 24, 100252. 10.1016/j.wroa.2024.100252.

Kang DD, Li F, Kirton E, Thomas A, Egan R, An H, Wang Z, 2019. MetaBAT 2: an adaptive binning algorithm for robust and efficient genome reconstruction from metagenome assemblies. Peer J 7, e7359. 10.7717/peerj.7359. [PubMed: 31388474]

Kehoe DM, 2010. Chromatic adaptation and the evolution of light color sensing in cyanobacteria. PNAS 107 (20), 9029–9030. 10.1073/pnas.1004510107. [PubMed: 20457899]

Kelly LT, Wood SA, McAllister TG, Ryan KG, 2018. Development and application of a quantitative PCR assay to assess genotype dynamics and anatoxin content in Microcoleus autumnalis-dominated mats. Toxins (Basel) 10 (11), 431. 10.3390/toxins10110431. [PubMed: 30373141]

Kelly LT, Bouma-Gregson K, Puddick J, Fadness R, Ryan KG, Davis TW, Wood SA, 2019. Multiple cyanotoxin congeners produced by sub-dominant cyanobacterial taxa in riverine cyanobacterial and algal mats. PLoS. One. 14 (2), e0220422. 10.1371/journal.pone.0220422. [PubMed: 31841562]

Kelly LT, Puddick J, Ryan KG, Champeau O, Wood SA, 2020. An ecotoxicological assessment of the acute toxicity of anatoxin congeners on New Zealand deleatidium species (mayflies). Inland. Waters. 10 (1), 101–108. 10.1080/20442041.2019.1626151.

Komárek J, Anagnostidis K, 2005. Cyanoprokaryota: oscillatoriales. In: Büdel B, Gärtner G, Krienitz L, Schagerl M (Eds.), Süsswasserflora Von Mitteleuropa 19/2. Elsevier, München.

Kormas KA, Lymperopoulou DS, 2013. Cyanobacterial toxin degrading bacteria: who are they? Biomed. Res. Int. 2, 463894. 10.1155/2013/463894.

Kust A, Méjean A, Ploux O, 2020. Biosynthesis of anatoxins in cyanobacteria: identification of the carboxy-anatoxins as the penultimate biosynthetic intermediates. J. Nat. Prod. 83, 142–151. 10.1021/acs.jnatprod.9b01121. [PubMed: 31899634]

Li X, Li L, Huang Y, Wu H, Sheng S, Jiang X, Chen X, Ostrovsky I, 2024. Upstream nitrogen availability determines the Microcystis salt tolerance and influences microcystins release in brackish water. Water. Res. 252, 121213. 10.1016/j.watres.2024.121213. [PubMed: 38306752]

McAllister TG, Wood SA, Hawes I, 2016. The rise of toxic benthic *Phormidium* proliferations: a review of their taxonomy, distribution, toxin content and factors regulating prevalence and increased severity. Harmful. Algae. 55, 282–294. 10.1016/j.hal.2016.04.002. [PubMed: 28073542]

McAllister TG, Wood SA, Greenwood MJ, Broghammer I, Hawes I, 2018. The effects of velocity and nitrate on Phormidium accrual cycles: a stream mesocosm experiment. Freshw. Sci. 37 (3), 496–501. 10.1086/699204.

Méjean A, Mann S, Maldiney T, Vassiliadis G, Lequin O, Ploux O, 2009. Evidence that biosynthesis of the neurotoxic alkaloids anatoxin-a and homoanatoxin-a in the cyanobacterium Oscillatoria PCC 6506 occurs on a modular polyketide synthase initiated by Ll-proline. J. Am. Chem. Soc. 131, 7512–7513. 10.1021/ja9024353. [PubMed: 19489636]

Méjean A, Mann S, Vassiliadis G, Lombard B, Loew D, Ploux O, 2010. In vitro reconstitution of the first steps of anatoxin-a biosynthesis in Oscillatoria PCC 6506: from free Ll-proline to acyl carrier protein bound dehydroproline. Biochem. (Basel) 49, 103–113. 10.1021/bi9018785.

Méjean A, Paci G, Gautier V, Ploux O, 2014. Biosynthesis of anatoxin-a and analogues (anatoxins) in cyanobacteria. Toxicon. 91, 15–22. 10.1016/j.toxicon.2014.07.016. [PubMed: 25108149]

Méjean A, Dalle K, Paci G, Bouchonnet S, Mann S, Pichon V, Ploux O, 2016. Dihydroanatoxin-a is biosynthesized from proline in *Cylindrospermum stagnale* PCC 7417: isotopic incorporation experiments and mass spectrometry analysis. J. Nat. Prod. 79, 1775–1782. 10.1021/acs.jnatprod.6b00189. [PubMed: 27340731]

Miller MB, Bassler BL, 2001. Quorum sensing in bacteria. Annu. Rev. Microbiol. 55, 165–199. 10.1146/annurev.micro.55.1.165. [PubMed: 11544353]

Mora D, Stancheva R, Abarca N, Bouchez A, Cantoral-Uriza E, Carmona-Jiménez J, Chonova T, Kusber W-H, Rimet F, Skibbe O, Wetzel CE, Zimmermann J, R., Jahn, R., 2024. Adding more taxa to the Cocconeis placentula (Bacillariophyta) group: two new species from streams in biodiversity hotspots. Nova Hedwig. 118, 277–319. 10.1127/nova_hedwigia/2024/0918.

Nguyen LT, Schmidt HA, von Haeseler A, Minh BQ, 2015. IQ-TREE: a fast and effective stochastic algorithm for estimating maximum-likelihood phylogenies. Mol. Biol. Evol. 32 (1), 268–274. 10.1093/molbev/msu300. [PubMed: 25371430]

Park H, Watanabe MF, Harada K, Nagai H, Suzuki M, Watanabe M, Hayashi H, 1993. Hepatotoxin (microcystin) and neurotoxin (anatoxin-a) contained in natural blooms and strains of cyanobacteria from Japanese freshwaters. Nat. Toxins. 1 (6), 353–360. [PubMed: 8167957]

Parks DH, Imelfort M, Skennerton CT, Hugenholtz P, Tyson GW, 2015. CheckM: assessing the quality of microbial genomes recovered from isolates, single cells, and metagenomes. Genome Res. 25, 1043–1055. http://www.genome.org/cgi/doi/10.1101/gr.186072.114. [PubMed: 25977477]

Pearl HW, Fulton RS III, Moisander PH, Dyble J, 2001. Harmful freshwater algal blooms, with an emphasis on cyanobacteria. TWSJ. 1, 76–113.

Perni S, Andrew PW, Sharma G, 2005. Estimating the maximum growth rate from microbial growth curves: definition is everything. Food Microbiol. 22 (6), 491–495. 10.1016/j.fm.2004.11.014.

Plato-Calzado C, Prieto A, Cameán AM, Jos A, 2022. Toxic effects produced by anatoxin-a under laboratory conditions: a review. Toxins (Basel) 14 (12), 861. 10.3390/toxins14120861. [PubMed: 36548758]

Puddick J, van Ginkel R, Page CD, Murray JS, Greenhough HE, Bowater J, Selwood AI, Wood SA, Prinsep MR, Truman P, Munday R, Finch SC, 2021. Acute toxicity of dihydroanatoxin-a from *Microcoleus autumnalis* in comparison to anatoxin-a. Chemosphere. 263, 127937. 10.1016/j.chemosphere.2020.127937. [PubMed: 32828056]

Puschner B, Hoff B, Tor ER, 2008. Diagnosis of anatoxin-a poisoning in dogs from North America. J. Vet. Diagn. Invest. 20, 89–92. 10.1177/104063870802000119. [PubMed: 18182518]

Quiblier C, Wood S, Echenique-Subiabre I, Heath M, Villeneuve A, Humbert J, 2013. A review of current knowledge on toxic benthic freshwater cyanobacteria e ecology, toxin production and risk management. Water. Res. 47, 5464–5479. 10.1016/j.watres.2013.06.042. [PubMed: 23891539]

Rantala-Ylinen A, Känä S, Wang H, Rouhiainen L, Wahlsten M, Rizzi E, Berg K, Gugger M, Sivonen K, 2011. Anatoxin-a synthetase gene cluster of the cyanobacterium Anabaena sp. Strain 37 and molecular methods to detect potential producers. AEM. 77 (20), 7271–7278. 10.1128/AEM.06022-11.

R Core Team, 2024. R: A language and Environment For Statistical Computing [online]. R Foundation for Statistical Computing, Vienna [viewed 12 March 2024]Available from. https://www.R-project.org/.

Schagerl M, Siedler R, Konopáčová E, Ali SS, 2022. Estimating biomass and vitality of microalgae for monitoring cultures: a roadmap for reliable measurements. Cells. 11 (15), 2455. 10.3390/cells11152455. [PubMed: 35954299]

Sinha R, Pearson LA, Davis TW, Muenchhoff J, Pratama R, Jex A, Burford MA, Neial BA, 2014. Comparative genomics of *Cylindrospermopsis raciborskii* strains with differential toxicities. BMC. Genomics. 15, 83. 10.1186/1471-2164-15-83. [PubMed: 24476316]

Skoupý S, Stanojković A, Cassamatta DA, McGovern C, Martinović A, Jaskowiec J, Konderlová M, Dodoková V, Mikesková P, Jahodářová E, Jungblut AD, van Schalkwyk H, Dvořak P, 2024. Population genomics and morphological data bridge the centuries of cyanobacterial taxonomy along the continuum of *Microcoleus* species. iScience. 27, 109444. 10.1016/j.isci.2024.109444. [PubMed: 38550993]

Smith C, Sutton A, 1993. Persistence of anatoxin-a in reservoir water. FWR Report No. FR0427. Available from: http://www.fwr.org/waterq/fr0427.htm.

Smith ZJ, Conroe DW, Schulz KL, Boyer GL, 2020. Limnological differences in a two-basin lake help to explain the occurrence of anatoxin-a, paralytic shellfish poisoning toxins, and microcystins. Toxins (Basel) 12 (9), 559. 10.3390/toxins12090559. [PubMed: 32872651]

Stancheva R, 2019. *Cocconeis cascadensis*, a new monoraphid diatom from mountain streams in Northern California, USA. Diatom. Res. 33 (4), 471–483. 10.1080/0269249X.2019.1571531.

Stancheva R, Brown S, Boyer GL, Wei B, Goel R, Henry S, Kristan NV, Read B, 2024. Effect of salinity stress and nitrogen depletion on growth, morphology and toxin production of freshwater cyanobacterium *Microcoleus anatoxicus* Stancheva & Conklin. Hydrobiologia. 10.1007/s10750-024-05586-3.

Stevens DK, Krieger RI, 1991. Stability studies on cyanobacterial nicotinic alkaloid anatoxin-a. Toxicon. 92 (2), 167–179. 10.1016/0041-0101(91)90101-V.

Stevenson RJ, Bahls LL, 1999. Periphyton protocols. In: Barbour MT, Gerritsen J, Snyder BD (Eds.), Rapid Bioassessment Protocols For Use in Wadeable Streams and Rivers: Periphyton, Benthic Macroinvertebrates, and Fish. United States Environmental Protection Agency, Washington, DC. EPA 841-B-99-002.

Strunecký O, Komárek J, Johansen J, Lukešová A, Elster J, 2013. Molecular and morphological criteria for the revision of the *genus Microcoleus* (Oscillatoriales, Cyanobacteria). J. Phycol. 49, 1167–1180. 10.1111/jpy.12128. [PubMed: 27007635]

Tee HS, Wood SA, Bouma-Gregson B, Lear G, Handley KM, 2021. Genome streamlining, plasticity, and metabolic versatility distinguish co-occurring toxic and nontoxic cyanobacterial strains of Microcoleus. mBio. 12, e02235. 10.1128/mBio.02235-21.-21. [PubMed: 34700377]

Testai E, 2021. Anatoxin-a and analogues. In: Chorus I, Welker M (Eds.), Toxic Cyanobacteria in Water, 2nd edition. CRC Press, Boca RatonFL, pp. 72–93. on behalf of the World Health Organization, Geneva, CH.

Toprowska M, Pawlik-Skowrońska B, Kalinowska R, 2014. Accumulation and effects of cyanobacterial microcystins and anatoxin-aon benthic larvae of Chironomus spp. (Diptera: chironomidae). Eur. J. Entomol. 111 (1), 83–90. 10.14411/eje.2014.010.

Stan Development Team. 2024. RStan: the R interface to Stan. R package version 2.21.2.

United States Environmental Protection Agency, 2015. Health Effects Support Document For the Cyanobacterial Toxin anatoxin-a. Document number 820R15104. Washington, DC, USA.

USGS, 2016. Long-Term Water Quality Monitoring Program in Upper Klamath Lake. Oregon. Accessed from. https://or.water.usgs.gov/projs_dir/klamath_ltmon/.

Valadez-Cano, Reyes-Prieto A, Beach DG, Rafuse C, McCarron P, Lawrence J, 2023. Genomic characterization of coexisting anatoxin-producing and non-toxigenic *Microcoleus* subspecies in benthic mats from the Wolastoq, New Brunswick, Canada. Harmful. Algae. 124, 102405. 10.1016/j.hal.2023.102405. [PubMed: 37164558]

van Appeldorn ME, van Egmond HP, Speijers GJA, Bakker GJI, 2007. Toxins of cyanobacteria. Mol. Nutr. Food Res. 51, 7–60. 10.1002/mnfr.200600185. [PubMed: 17195276]

Wang J, Guo X, 2024. The Gompertz model and its applications in microbial growth and bioproduction kinetics: past, present and future. Biotechnol. Adv. 72, 108335. 10.1016/j.biotechadv.2024.108335. [PubMed: 38417562]

Weigel BL, Welter JR, Fuery P, 2020. Invertebrate grazing and epilithon assemblages control benthic nitrogen fixation in an N-limited river network. Freshw. Sci. 39, 508–520. 10.1086/710023.

Wickham H, Chang W, Henry L, Pederson TL, Takahashi K, Wilke C, Woo K, Yutani HD Dunnington. ggplot2: create elegant data visualizations using the grammar of graphics. In: R package version 4.3.2. 2016.

World Health Organization, 2020. Cyanobacterial toxins: Anatoxin-A and Analogues. Geneva, Switzerland.

Wood SA, Selwood AI, Rueckert A, Holland PT, Milne JR, Smith KF, Smits B, Watts LF, Cary CS, 2007. First report of homoanatoxin-a and associated dog neurotoxicosis in New Zealand. Toxicon. 50, 292–301. 10.1016/j.toxicon.2007.03.025. [PubMed: 17517427]

Wood SA, Smith FJM, Heath MW, Palfroy T, Gaw S, Young RG, Ryan KG, 2012. Within-mat variability in anatoxin-a and homoanatoxin-a production among benthic Phormidium (Cyanobacteria) strains. Toxins (Basel) 4, 900–912. 10.3390/toxins4100900. [PubMed: 23162704]

Wood SA, Atalah J, Wagenhoff A, Brown L, Doehring K, Young RG, Hawes I, 2017. Effect of river flow, temperature, and water chemistry on proliferations of the benthic anatoxin-producing cyanobacterium *Phormidium*. Freshw. Sci. 36 (1), 63–76. 10.1086/690114.

Wood SA, Puddick J, 2017. The abundance of toxic genotypes is a key contributor to anatoxin variability in *Phormidium*-dominated benthic mats. Mar. Drugs. 15, 307. 10.3390/md15100307. [PubMed: 29019928]

Wood SA, Biessy L, Puddick J, 2018. Anatoxins are consisyently released into the water of streams with Microcoleus autumnalis-dominated (cyanobacteria) proliferations. Harmful. Algae. 80, 88–95. 10.1016/j.hal.2018.10.001. [PubMed: 30502816]

Wood SA, Kelly LT, Bouma-Gregson K, Humbert J, Laughinghouse IV HD, Lazorchak J, McAllister TG, McQueen A, Pokrzywinski K, Puddick J, Quiblier C, Reitz L, Ryan KG, Vadeboncoeur Y, Zastepa A, Davis TW, 2020. Toxic benthic freshwater cyanobacterial proliferations: challenges and solutions for enhancing knowledge and improving monitoring and mitigation. Freshw. Biol. 65 (10), 1824–1842. 10.1111/fwb.13532. [PubMed: 34970014]

Yang X, 2007. Occurrence of the Cyanobacterial Neurotoxin, Anatoxin-a, in New York State waters, 245. State University of New York, College of Environmental Science and Forestry. UMI Number 3290535.

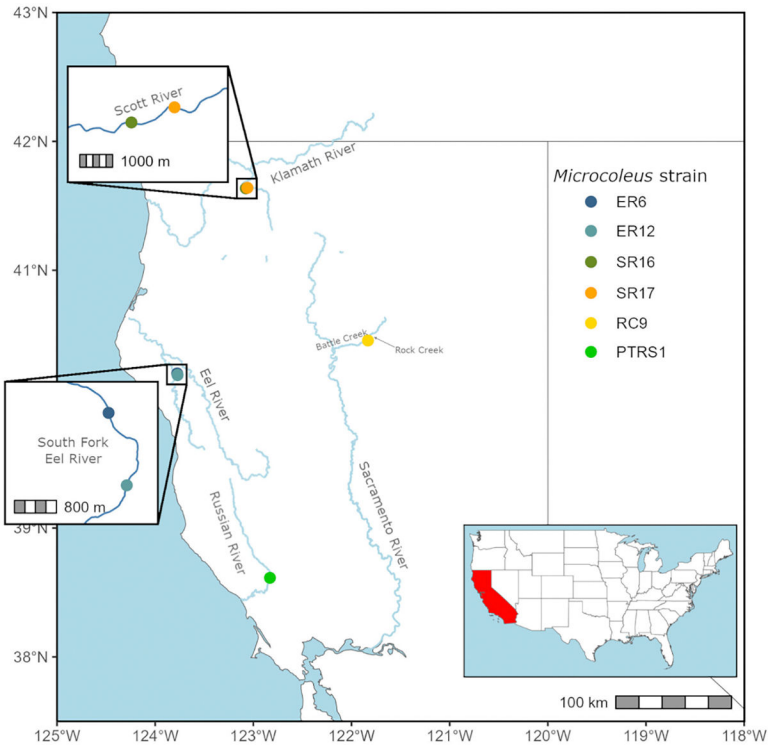

Fig. 1.

Streams in California where each *Microcoleus* strain was isolated from.

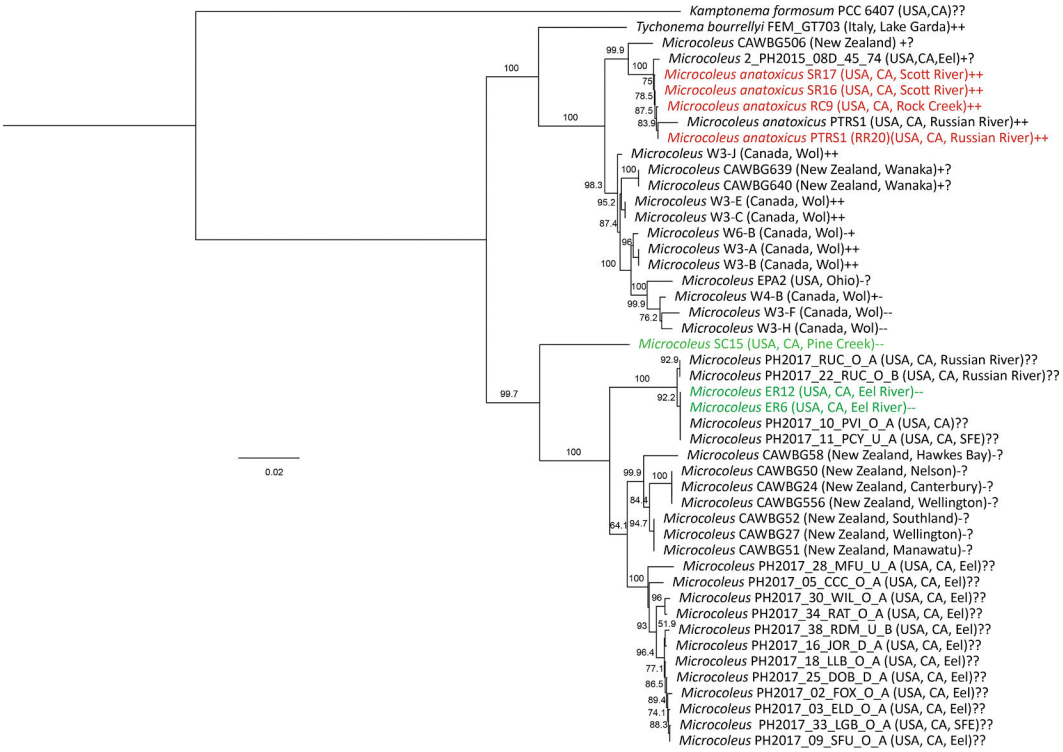

Fig. 2.

Phylogenetic tree of cyanobacterial MAGs including studied *Microcoleus* strains from northern California (color coded-toxic strains in red, non-toxic strains in green) using 120 core genes. Strain name is listed with collection locality (See Supplemental Table 1 for more information). The pair of plus and minus signs after the strain name indicates the test results for presence of ATX gene cassette (first symbol) and anatoxin production measured by LC-MS/MS (second symbol). (+ +) denotes presence of both ATX gene cassette and ATX toxin(s); (+ −) denotes presence of ATX gene cassette and lack of ATX toxin(s); (− +) denotes absence of ATX gene cassette but detection of ATX toxins(s), (− −) denotes absence of ATX gene cassette and lack of ATX toxin(s), (?) indicates that data was unavailable in the literature, e. g., strains were not tested.

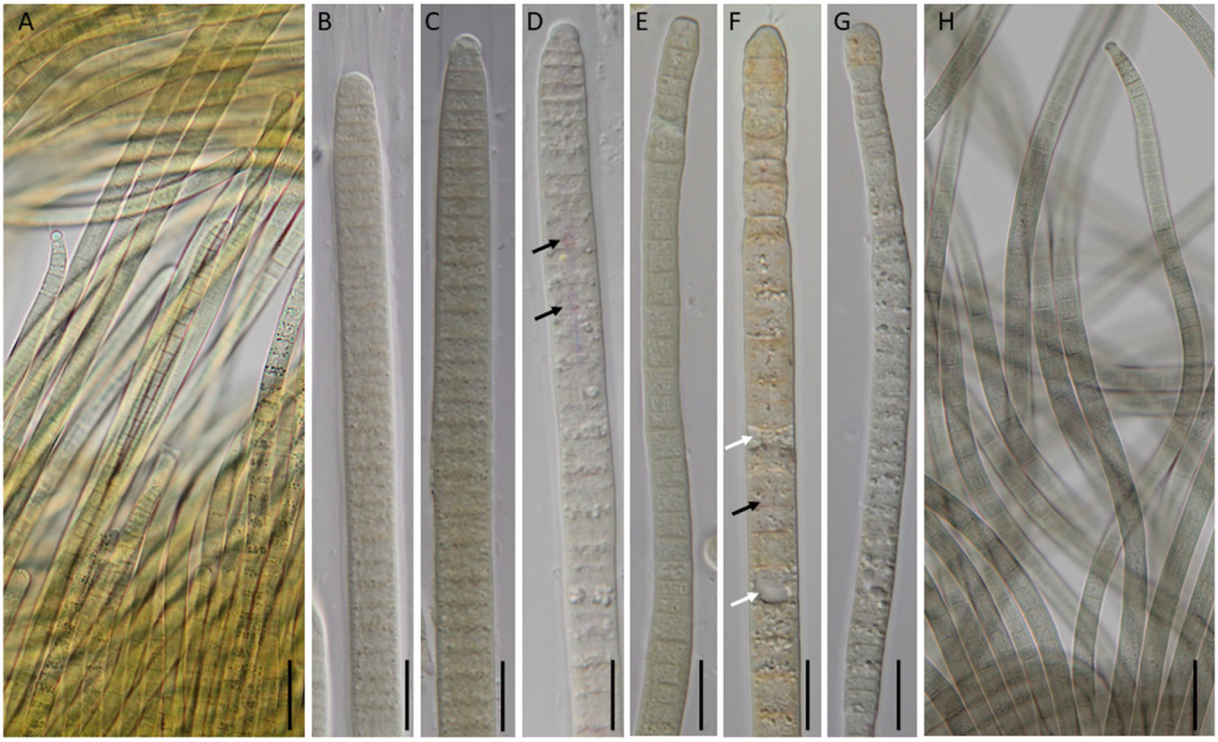

Fig. 3.

Light microscopy images of *Microcoleus* filaments from field mats (A and H) and after 40 days growth in batch cultures with BG11 (B-G). A, B. *Microcoleus* sp. 1 strain ER6 from Eel River, C. *Microcoleus* sp. 1 strain ER12, D. *M. anatoxicus* strain SR16, E. *M. anatoxicus* strain SR17, F. *M. anatoxicus* strain PTRS1, G, H. *M. anatoxicus* strain RC9 from Rock Creek. Black arrows indicate ruptures in the cells walls and leaking of pigments; white arrows indicate keritomized cells. Images B - C were obtained at 1000x using differential interference contrast (DIC) microscopy, while images A and H were obtained at 400x without DIC. Sale bar = 10 μm for B - G; 20 μm for A and H. **Note:** Strains SR16 and PTRS1 are more toxic while strains SR17 and RC9 are less toxic.

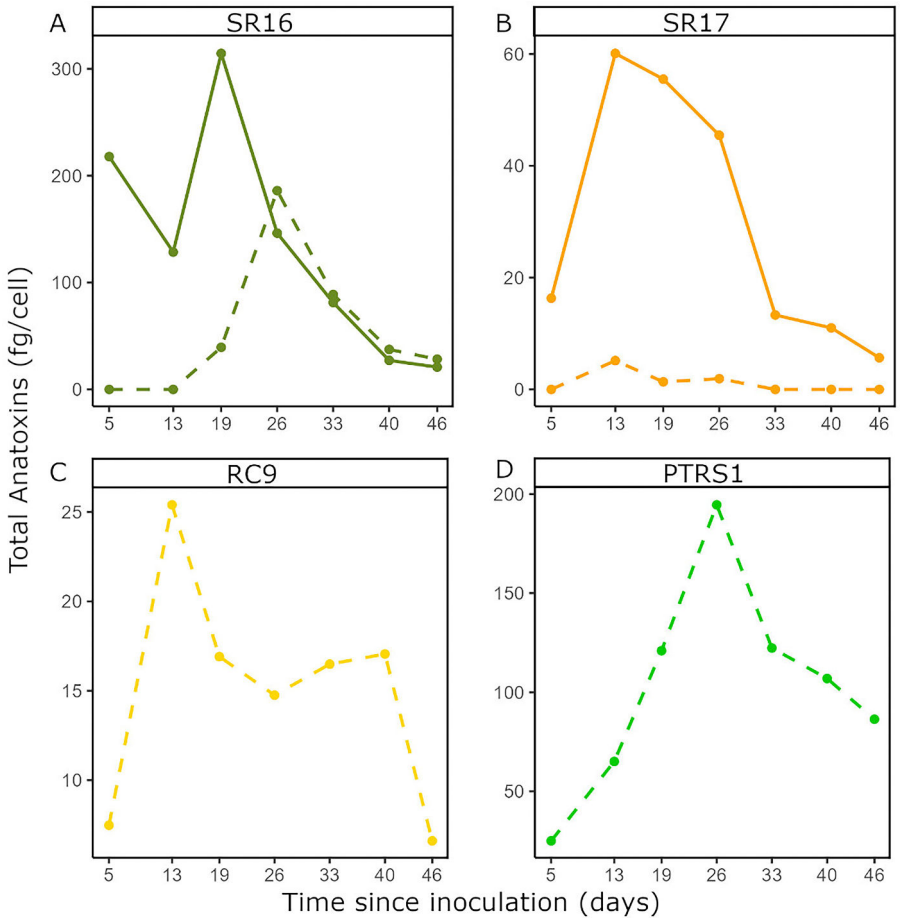

Fig. 4.

Curves generated for *Microcoleus* toxin quotas (intracellular + extracellular anatoxins) across time. Solid lines signify ATX and dashed lines signify dhATX. Points represent the average toxin concentration per cell. A. *Microcoleus anatoxicus* strain SR16, B. *M. anatoxicus* strain SR17, C. *M. anatoxicus* strain RC9, and D. *M. anatoxicus* strain PTRS1. **Note:** Strains SR16 and PTRS1 are more toxic while strains SR17 and RC9 are less toxic.

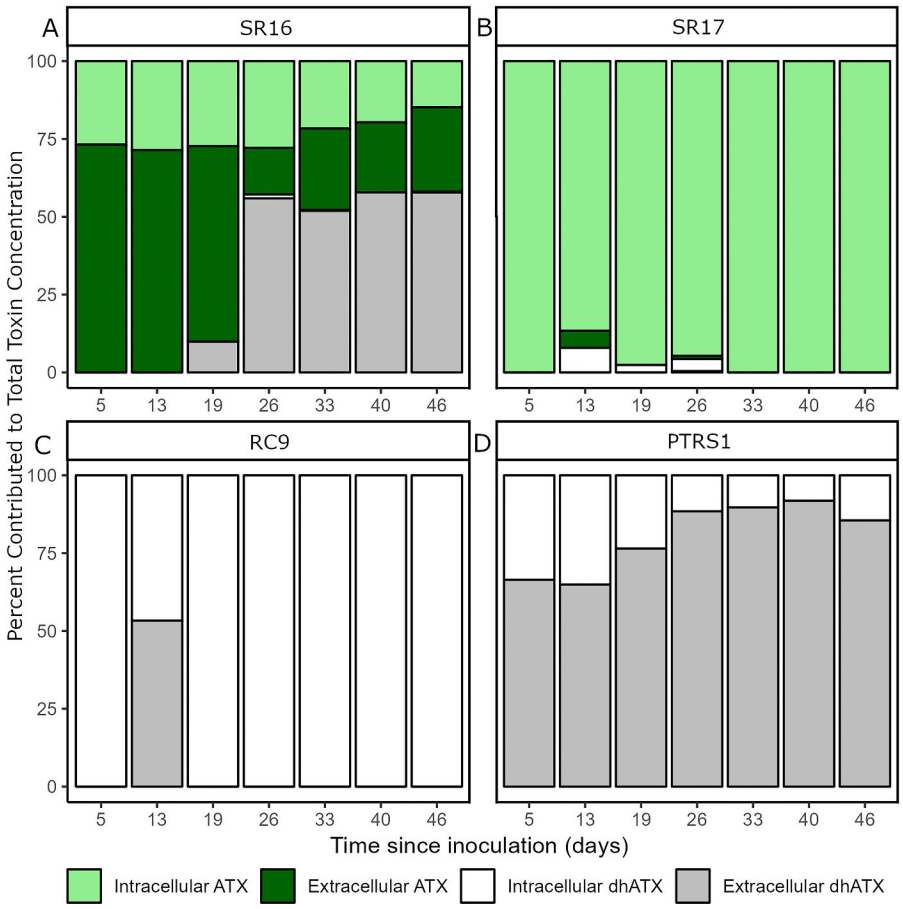

Fig. 5.

Proportion of intracellular and extracellular ATX and dhATX fractions for each *Microcoleus* strain for each harvest period, bars represent average duplicate values for each toxin fraction measured through time. A. *Microcoleus anatoxicus* strain SR16, B. *M. anatoxicus* strain SR17, C. *M. anatoxicus* strain RC9, and D. *M. anatoxicus* strain PTRS1. **Note:** Strains SR16 and PTRS1 are more toxic while strains SR17 and RC9 are less toxic.

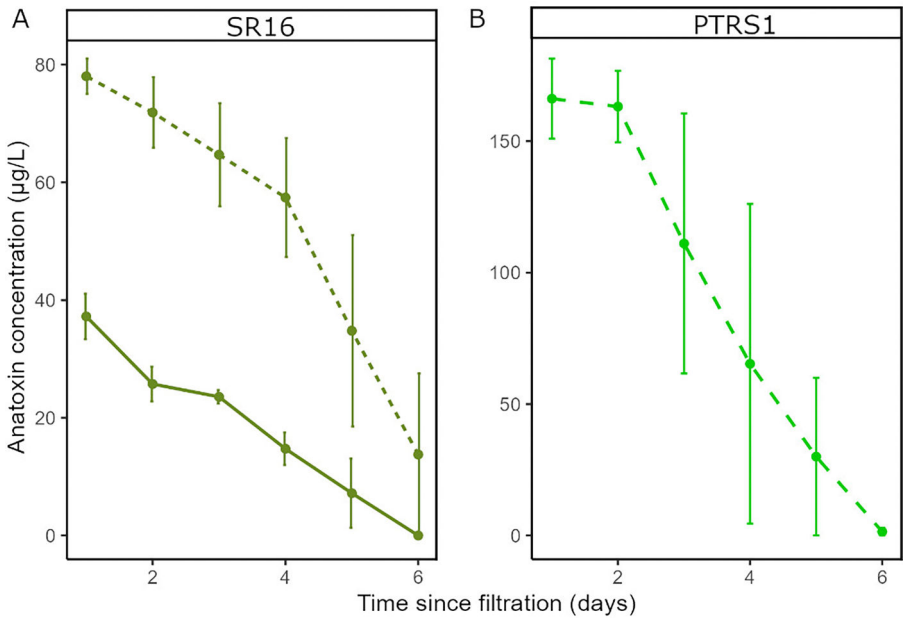

Fig. 6.

Degradation of ATX and dhATX under standard laboratory conditions and natural room light in the filtered liquid from *Microcoleus anatoxicus* strains SR16 (A) and *Microcoleus anatoxicus* PTRS1 (B). Solid line represents ATX concentration and dashed line represents dhATX concentrations through time. Points signify the mean values with error bars denoting the maximum and minimum recorded anatoxin concentrations from the duplicates. **Note:** Strains SR16 and PTRS1 are more toxic.

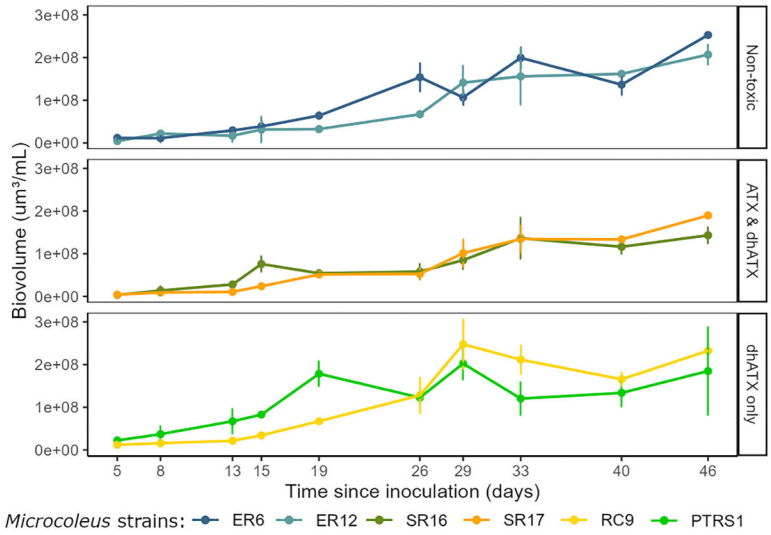

Fig. 7.

Curves of all *Microcoleus* strains based on data collected for biovolume density, grouped by number of anatoxin-a variants produced. Points signify mean of biovolume density values ± standard deviation. Biovolume calculations were estimated based off of Hillebrand et al. (1999, see Section 2.5). Averages calculated from triplicate biovolume values and their respective standard deviations. **Note:** Strains SR16 and PTRS1 are more toxic while strains SR17 and RC9 are less toxic.

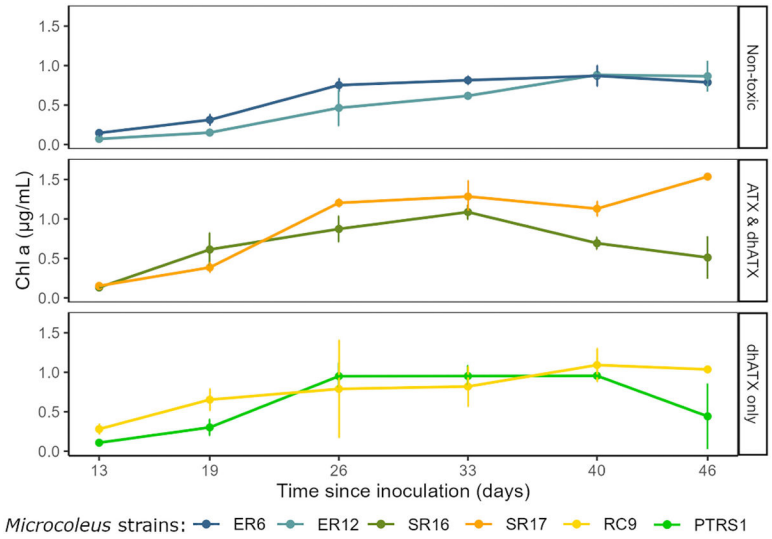

Fig. 8.

Curves of all *Microcoleus* strains based on data collected for chlorophyll *a*, grouped by number of anatoxin-a variants produced. Points signify mean of chlorophyll *a* values ± standard deviation. Averages calculated from duplicate chlorophyll *a* values and their respective standard deviations. **Note:** Strains SR16 and PTRS1 are more toxic while strains SR17 and RC9 are less toxic.

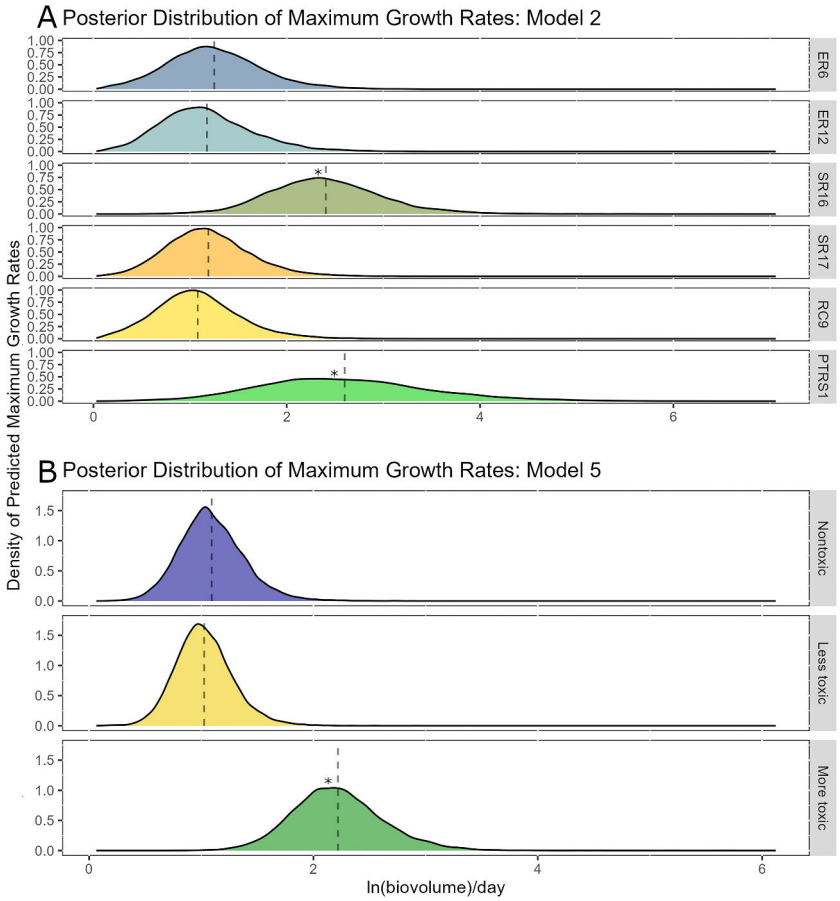

Fig. 9.

Posterior probability distributions of the maximum growth rates of strains based on model 2 (A) where all strains were split and model 5 (B) where strains were pooled by the concentration of toxins produced during peak toxin production (non-toxic versus high concentrations versus low concentrations). **Note:** Strains SR16 and PTRS1 are more toxic, as indicated by *, while strains SR17 and RC9 are less toxic.

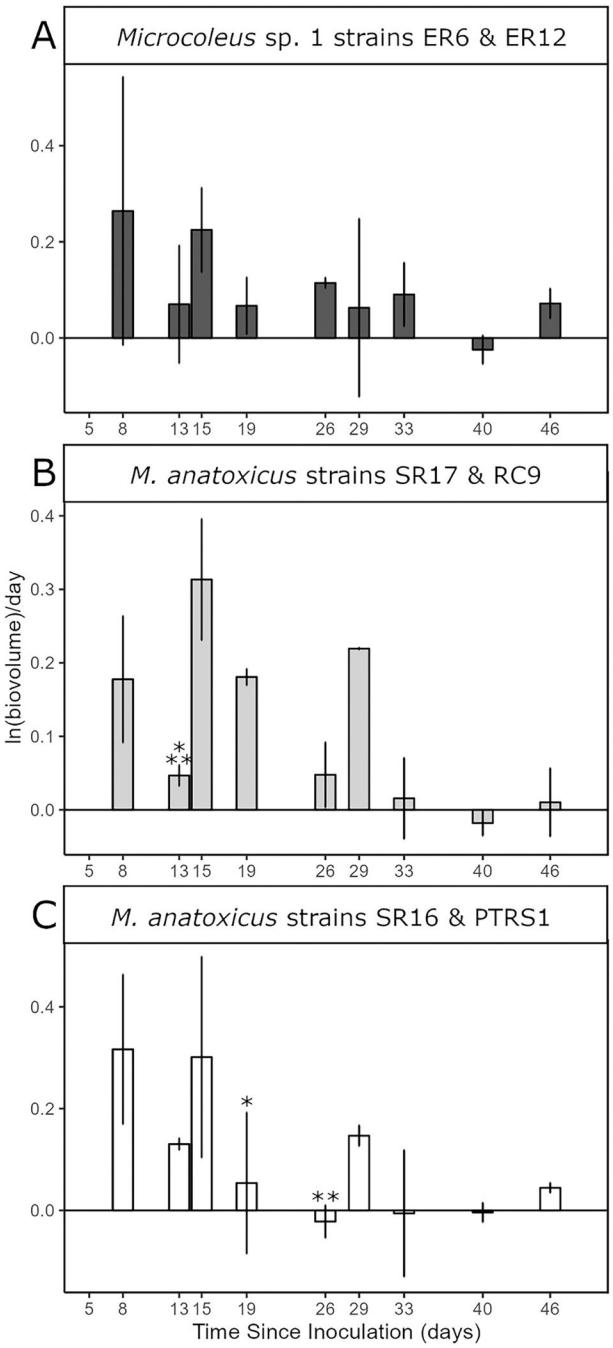

Fig. 10.

Specific growth rate of *Microcoleus* strains between each harvest period (x-axis). Bars represent the average values between the two strains and the error bars represent the standard deviation. A. Non-toxic *Microcoleus* strains ER6 and ER12; B. Toxic *Microcoleus* strains producing dhATX and ATX, SR16 and SR17; C. Toxic *Microcoleus* strains producing dhATX only, RC9 and PTRS1. (*) denotes peak ATX production, (**) denotes peak dhATX

production. **Note:** Strains SR16 and PTRS1 are more toxic while strains SR17 and RC9 are less toxic.

Table 1

Microcoleus strains used in the experiment with locality data and selected environmental variables at the time of their collection for isolation.

Stream	Strains Isolated	Date Sampled	Coordinates	Water discharge (m^3/m)	Temperature (°C)	pH	PO_4-P (mg/L)	NO_3-N (mg/L)	Total Phosphorus (mg/L)	Total Nitrogen (mg/L)
South Fork Eel River	ER6, ER12	8/23/2022	40.19922756, −123.776087; 40.186918, −123.772014	0.75–0.78	24.2–24.7	8.62–8.75	0.0038–0.0042	0.015–0.018	NA	NA
Scott River	SR16, SR17	9/20/2022	41.63569722, −123.07645; 41.63983889, −123.0606861	NA	NA	NA	NA	NA	NA	NA
Rock Creek	RC9	10/7/2020	40.4548, −121.833	NA	6	7.7–9.3	NA	NA	below 0.08	below 0.1
Russian River	PTRS1	10/1/2015	38.613618, −122.831158	NA	NA	NA	NA	NA	0.0096	0.151

NA= no data available.

Table 2

Different Gompertz Model assignments of matching growth rates to respective strains. The different models were employed to test the hypothesis of which strains achieved the fastest maximum growth rates.

Model	Strains Growth Rate Groups
1	(ER6 + ER12 + **SR16*** + *SR17** + *RC9*$^{+}$ + **PTRS1**$^{+}$)
2	(ER6) ≠ (ER12) ≠ (**SR16***) ≠ (*SR17**) ≠ (*RC9*$^{+}$) ≠ (**PTRS1**$^{+}$)
3	(ER6 + ER12) ≠ (**SR16*** + *SR17** + *RC9*$^{+}$ + **PTRS1**$^{+}$)
4	(ER6 + ER12) ≠ (**SR16*** + *SR17**) ≠ (*RC9*$^{+}$ + **PTRS1**$^{+}$)
5	(ER6 + ER12) ≠ (**SR16*** + **PTRS1**$^{+}$) ≠ (*SR17** + *RC9*$^{+}$)

ER6 = *Microcoleus* sp. 1 strain ER6, ER12 = *Microcoleus* sp. 1 strain ER12, SR16 = *M. anatoxicus* strain SR16, SR17 = *M. anatoxicus* strain SR17, RC9 = *M. anatoxicus* strain RC9, PTRS1 = *M. anatoxicus* strain PTRS1. + indicates that strains were assigned the same growth rates. ≠ indicates that strains were assigned different growth rates. Italicized strains are less toxic, bolded strains are more toxic. (*) denotes that the strain produces both ATX and dhATX, ($^{+}$) denotes that the strains produce dhATX only.

Table 3

WAIC values for each model run listed from best fitting model to the worst. $ELPD_{WAIC}$ is the expected log pointwise predictive density using the widely available information criterion. p_{WAIC} is effective number of parameters, SE is standard error of each measurement.

Model	WAIC	SE	$ELPD_{WAIC}$	SE	p_{WAIC}	SE
5	222.1	24.9	−111.1	12.4	28.5	4.0
1	225.2	24.3	−112.6	12.1	30.2	4.0
3	228.8	24.1	−114.4	12.0	32.2	12.0
4	231.7	24.1	−115.9	12.1	33.8	4.3
2	236.1	25.7	−118.1	12.8	36.3	5.0

Table 4

Predicted mean and standard error (SE) of maximum growth rate outputs from Gompertz models 2 and 5.

Predicted Maximum Growth Rates		
Model 2		
Strain	**Mean of ln(biovolume)/day**	**SE**
ER6	1.25	0.01
ER12	1.17	0.01
SR16*	2.41	0.01
SR17*	1.19	0.01
RC9^{+}	1.08	0.01
PTRS1^{+}	2.60	0.01
Model 5		
ER6 + ER12	1.09	0.01
SR17* + *RC9*$^{+}$	1.02	0.01
SR16* + **PTRS1**$^{+}$	2.21	0.01

ER6 = *Microcoleus* sp. 1 strain ER6, ER12 = *Microcoleus* sp. 1 strain ER12, SR16 = *M. anatoxicus* strain SR16, SR17 = *M. anatoxicus* strain SR17, RC9 = *M. anatoxicus* strain RC9, PTRS1 = *M. anatoxicus* strain PTRS1. Italicized strains are less toxic, bolded strains are more toxic. (*) denotes that the strain produces both ATX and dhATX, ($^{+}$) denotes that the strains produce dhATX only.